Overview of Code-Domain Power, Timing, and Phase Measurements

Telecommunications Industry Association standards specify various measurements designed to ensure the compatibility of North American CDMA (code division multiple access) cellular transmitters and receivers. This paper is a tutorial overview of the operation of the measurement algorithms in the HP 83203B CDMA cellular adapter, which is designed to make the base station transmitter measurements specified in the standards.

by Raymond A. Birgenheier

In 1994, the Telecommunications Industry Association (TIA) released the IS-95 and IS-97 standards developed by the TIA TR-45.5 subcommittee. These standards ensure the mobile-station/base-station compatibility of a dual-mode wideband spread spectrum system—the North American CDMA (code division multiple access) cellular telephone system.[1] CDMA is a class of modulation that uses specialized codes to provide multiple communication channels in a designated segment of the electromagnetic spectrum. The TIA IS-95/97 standards specify various measurements that must be made on CDMA base station and mobile station transmitters and receivers to ensure their compatibility. The HP 83203B CDMA cellular adapter for the HP 8921A Option 600 cell site test system is designed to make the base station transmitter measurements specified in the standards. The HP 83203B algorithms provide accurate measurements of code-domain power, time, frequency, and phase. This paper is a tutorial overview of the operation of the measurement algorithms in the HP 83203B.

The HP 83203B measurement algorithms provide a characterization of the code-domain channels of a CDMA base station transmitter. One of the measurements, called code-domain power, provides the distribution of power in the code channels. This measurement can be used to verify that the various channels are at expected power levels and to determine when one code channel is leaking energy into the other code channels. The crosscoupling of code channels can occur for many reasons. One reason is a time misalignment of the channels, which would negate the orthogonal relationship among code channels. Another reason may be the impairment of the signals caused by nonideal or malfunctioning components in the transmitter. To determine the quality of the transmitter signal, a waveform quality factor, ρ, is measured. It is the amount of transmitter signal energy that correlates with an ideal reference signal when only the pilot channel is transmitted.

Another set of measurements, called code-domain timing and code-domain phase, determine how well-aligned the code channels are in time and in phase. The parameters measured are time offsets and phase offsets of active code channels relative to the pilot channel (code channel 0).

To make these measurements to the precision specified in the IS-97 standard, it is necessary to establish the time origin and the carrier frequency of the signal to be measured. The HP 83203B provides these measurements. Another measurement that may be useful when diagnosing the causes of poor transmitter signal quality is the carrier feedthrough in the transmitter signal. The effect of carrier feedthrough will also be seen when measuring code-domain power.

This paper presents (1) the general concepts of CDMA signals and measurements, (2) the signal flow of the measurement algorithms, (3) the specifications from the IS-97 standard and performance predictions for the measurement algorithms based on mathematical modeling and simulations, and (4) some typical results of measurements made with the HP 83203B.

CDMA Operation

The channel structure for a CDMA base station transmitter is shown in Fig. 1. There are 64 code channels, corresponding to 64 Walsh functions, each 64 chips long.* To see how the Walsh functions provide the channelization, we will consider a hypothetical example of four code channels produced by the four orthogonal Walsh functions shown in Fig. 2. The sums shown in Fig. 1 are modulo-2, as defined in Table I. They are appropriate when a 0,1 representation is used for binary numbers and are equivalent to ordinary multiplication when a 1,–1 representation is used. The Walsh functions use nonreturn-to-zero (NRZ) values of 1 and –1 to represent binary numbers.

* The chip interval is the clock period of the spreading code used in a spread-spectrum system. In this paper, a chip corresponds to one binary digit of the pilot pseudonoise sequences shown in Fig. 1.

Fig. 1. *Forward CDMA (base station transmitter) channel structure.*

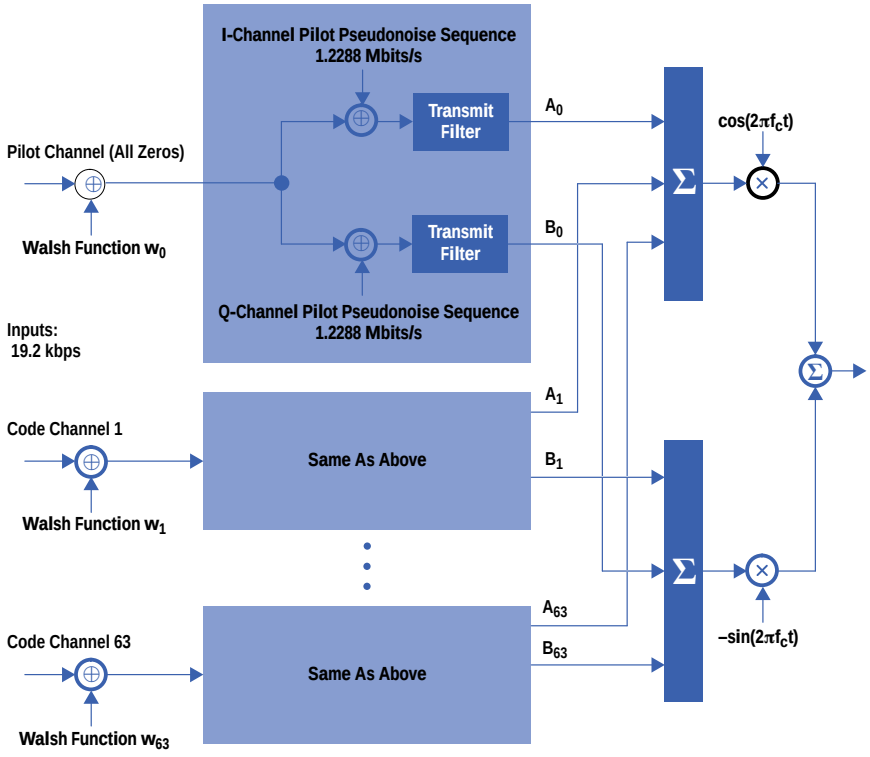

Table I
Modulo-2 Sum (XOR)

⊕	0	1
0	0	1
1	1	0

The Walsh functions are said to be orthogonal because the inner product of $w_i(t)$ and $w_j(t)$ is:

$$\int_0^4 w_i(t)w_j(t) = 4, \quad i = j \qquad (1)$$
$$= 0, \quad i \neq j$$

that is, the inner product of two distinct Walsh functions is zero.

The orthogonality property produces the channelization, as we can see by considering the transmission of a binary digit (bit) that is four chip intervals long on channel 1. If the bit is represented by ±1, then at the transmitter and, ideally, at the receiver the bit is represented by $\pm w_1(t)$. At the receiver, an operation equivalent to equation 1 is performed on $\pm w_1(t)w_i(t)$ for each channel for i = 0, 1, 2, 3. This operation produces the result:

$$\int_0^4 w_1(t)w_i(t) = \pm 4, \quad i = 1 \qquad (2)$$
$$= 0, \quad i \neq 1$$

Therefore, we see that the bit can be detected on channel 1, but it does not appear on channels 0, 2, or 3.

The 64 Walsh functions used for the channelization shown in Fig. 1 are represented by 64-bit words that are rows (or columns) of a 64×64 Hadamard matrix. The Hadamard matrix is orthogonal (i.e., rows or columns are orthogonal) and can be generated by the following simple algorithm:

- A 2×2 Hadamard matrix is defined as:

Fig. 2. *Four orthogonal Walsh functions.*

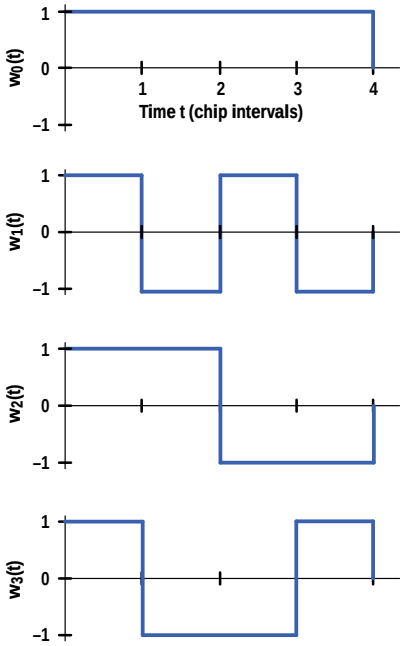

$$H_2 = \begin{bmatrix} 0 & 0 \\ 0 & 1 \end{bmatrix}. \qquad (3)$$

- A 4×4 Hadamard matrix is generated as:

$$H_4 = \begin{bmatrix} H_2 & H_2 \\ H_2 & \overline{H_2} \end{bmatrix} = \begin{bmatrix} 0 & 0 & 0 & 0 \\ 0 & 1 & 0 & 1 \\ 0 & 0 & 1 & 1 \\ 0 & 1 & 1 & 0 \end{bmatrix}. \qquad (4)$$

- In general, a Hadamard matrix H_{2n} is generated from a Hadamard matrix H_n by:

$$H_{2n} = \begin{bmatrix} H_n & H_n \\ H_n & \overline{H_n} \end{bmatrix}. \qquad (5)$$

The inner product of two rows of H_n is obtained by the modulo-2 summing of the two rows, element by element, and counting the difference between the number of 0s and 1s, where the modulo-2 sum is the XOR operation defined in Table I. For example, to obtain the inner product of rows 1 and 2 of H_4, we perform the following operation:

$$\begin{array}{cccccc} & 0 & 0 & 0 & 0 & \\ \oplus & 0 & 1 & 0 & 1 & \\ \hline & 0 & 1 & 0 & 1 & \Leftarrow \end{array} \qquad (6a)$$

Inner product = number of 0s minus number of 1s = 0

If a 1,–1 representation is used for the binary numbers, then the inner product given by equation 6a is simply:

$$\begin{array}{cccccc} & 1 & 1 & 1 & 1 & \\ \times & 1 & -1 & 1 & -1 & \\ \hline & 1 & -1 & 1 & -1 & \Leftarrow \end{array} \qquad (6b)$$

Inner product = sum = 0.

Fig. 3 shows an example of the pseudonoise encoding shown in Fig. 1 for code channel 1. The input bits, denoted by d_i, are added (modulo-2) to the Walsh function w_1 and then to the I-channel and Q-channel pseudonoise sequences i_{pn} and q_{pn}. The resulting modulo-2 sums are converted to ±1 for I_k and Q_k, where +1 represents binary 0 and –1 represents binary 1. The discrete time signals I_k and Q_k provide the inputs to the transmit filters. The outputs of these filters are the superposition of pulses centered at discrete times t_k, k = ..., 0, 1, 2, ..., as illustrated in Fig. 4.

If the pulse for I_k or Q_k equals zero when $t = t_i$, $i \neq k$, then the pulses at the outputs of the transmit filters do not interfere with each other at discrete times t_k, k = ..., 0, 1, 2, ... and we say the transmit filters introduce zero intersymbol interference.

Fig. 3. *Pseudonoise encoding.*

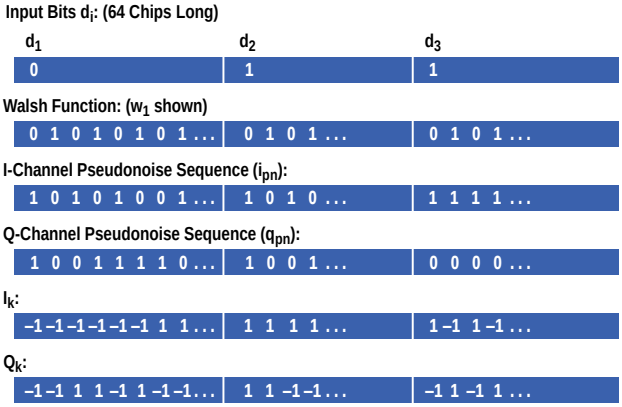

Fig. 4. *Transmit filter output.*

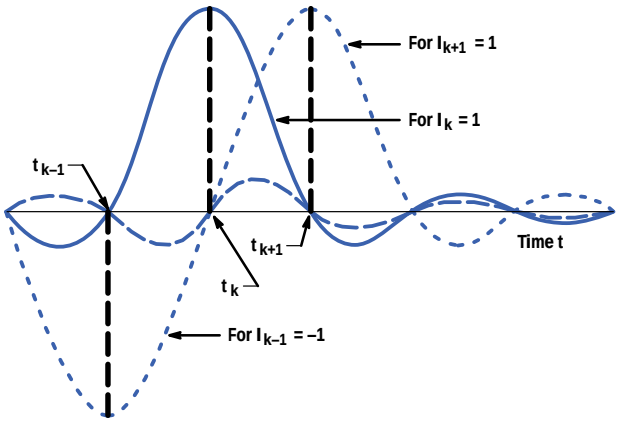

The transmit filters illustrated in Fig. 4 introduce zero intersymbol interference. However, the transmit filter specified in the IS-95 standard does introduce intersymbol interference. Moreover, the base station transmitter specified in the standard must incorporate an all-pass phase preequalizer, which produces an asymmetric transmitter pulse response.

The reason for the I-Q structure shown in Fig. 1 will become clearer after we consider code-domain signals.

Code-Domain Signals (Forward Link)

Any sinusoidal carrier with amplitude and phase modulation can be written mathematically as:

$$X(t) = A(t)\cos[\omega_c t + \Phi(t)] \qquad (7)$$

where $\omega_c = 2\pi f_c$ (f_c is the carrier frequency in Hz), $A(t)$ is the instantaneous amplitude, and $\Phi(t)$ is the instantaneous phase.

Using the trigonometric identity $\cos(\theta+\varphi) = \cos\theta\cos\varphi - \sin\theta\sin\varphi$, equation 7 can be rewritten as:

$$\begin{aligned} X(t) &= A(t)\cos\Phi(t)\cos\omega_c t - A(t)\sin\Phi(t)\sin\omega_c t \\ &= I(t)\cos\omega_c t - Q(t)\sin\omega_c t, \end{aligned} \qquad (8)$$

where the in-phase component of the signal (the component multiplying the carrier $\cos\omega_c t$) is:

$$I(t) = A(t)\cos\Phi(t), \qquad (9)$$

and the quadrature component (the component multiplying the quadrature carrier $-\sin\omega_c t$) is:

$$Q(t) = A(t)\sin\Phi(t). \qquad (10)$$

Using Euler's identity, $e^{j\theta} = \exp(j\theta) = \cos\theta + j\sin\theta$, we can write:

$$I(t) + jQ(t) = A(t)e^{j\Phi(t)}. \qquad (11)$$

$I(t)+jQ(t)$ is called the complex envelope of the modulated carrier and is represented as a rotating phasor as shown in Fig. 5. The tip of the rotating phasor moves as a function of time forming the locus referred to as the signal trajectory.

Fig. 5. *The complex envelope of the modulated carrier is represented as a rotating phasor. The locus of the tip of the phasor is called the signal trajectory.*

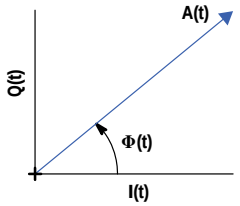

The forward link of the CDMA system uses quadrature phase-shift keying (QPSK) modulation. First, we will consider the case in which only the pilot signal is present. In this case, if no intersymbol interference is introduced by the transmit filter, the signal trajectory passes through four discrete points separated by multiples of 90 degrees in the I-Q plane as shown in Fig. 6. These four points on the I-Q diagram are referred to as the signal constellation for the QPSK modulation.

The coordinates of these points represent the four possible values of a pair of bits. As the signal moves along its trajectory, the coordinates at discrete time t_k represent the pair of bits transmitted at this time. The example signal trajectory presented in Fig. 6 is for the first eight pairs of bits of the pilot sequences with corresponding times t_k, as given in Table II.

Table II
First 8 Pairs of Bits of Pilot Sequences

k	1	2	3	4	5	6	7	8
i_{pn}	–1	1	–1	1	–1	1	1	–1
q_{pn}	–1	1	1	–1	–1	–1	–1	1

Now we will consider a case in which the pilot (code channel 0) and code channel 1 are transmitted simultaneously. In this case, the transmitter signal can be represented as:

$$X(t) = A_0(t)\cos\left[\omega_c t + \Phi_0(t)\right] + A_1(t)\cos\left[\omega_c t + \Phi_1(t)\right], \quad (12)$$

where $A_0(t)$ and $\Phi_0(t)$ represent the amplitude and phase modulation introduced by the pilot and $A_1(t)$ and $\Phi_1(t)$ represent the amplitude and phase modulation introduced by code channel 1. Using the trigonometric identity $\cos(\theta+\varphi) = \cos\theta\cos\varphi - \sin\theta\sin\varphi$, we can write equation 12 as:

$$\begin{aligned} X(t) &= \left[A_0(t)\cos\Phi_0(t) + A_1(t)\cos\Phi_1(t)\right]\cos(\omega_c t) \\ &\quad - \left[A_0(t)\sin\Phi_0(t) + A_1(t)\sin\Phi_1(t)\right]\sin(\omega_c t) \quad (13) \\ &= I(t)\cos(\omega_c t) - Q(t)\sin(\omega_c t), \end{aligned}$$

where

$$I(t) = A_0(t)\cos\Phi_0(t) + A_1(t)\cos\Phi_1(t) \quad (14)$$

and

$$Q(t) = A_0(t)\sin\Phi_0(t) + A_1(t)\sin\Phi_1(t). \quad (15)$$

From equations 14 and 15, it is clear that since

$$I(t) = I_0(t) + I_1(t) \text{ and } Q(t) = Q_0(t) + Q_1(t), \quad (16)$$

I(t) and Q(t) are simply the superposition of the corresponding components produced by the pilot and code channel 1. Therefore, we can superimpose I-Q diagrams.

To simplify the description at this point, we will consider the code channels produced by four orthogonal Walsh words each four chips long, as shown in Table III.

Table III
Orthogonal Walsh Words

w_0:	1	1	1	1
w_1:	1	–1	1	–1
w_2:	1	1	–1	–1
w_3:	1	–1	–1	1

For illustrative purposes, we will assume that the peak magnitude $\sqrt{2}\,a_0 = |A_0(t_k)|_{peak}$ of the pilot (code channel 0) is $0.8\sqrt{2}$ and the magnitude $\sqrt{2}\,a_1 = |A_1(t_k)|_{peak}$ of the signal for code channel 1 is $0.6\sqrt{2}$, so that the root-sum-square of the pilot and code channel 1 signals is:

$$\sqrt{0.8^2 + 0.6^2} = 1.0. \qquad (17)$$

In this case, the pilot signal has the trajectory shown in Fig. 6, except that the signal coordinates are (±0.8, ±0.8) instead of (±1, ±1).

Fig. 6. *Example of a signal constellation (points) and a signal trajectory.*

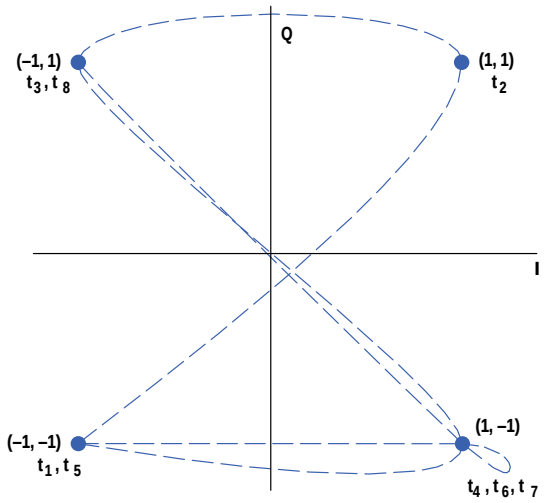

To determine the trajectory produced by code channel 1, we must consider multiplying Walsh word w_1 by data bits. For our example, we will assume data bits for two Walsh function intervals: d = 1, –1. We obtain values for I_1 and Q_1 as presented in Table IV.

Table IV
Calculation of I_1 and Q_1

Time	t_1	t_2	t_3	t_4	t_5	t_6	t_7	t_8
i_{pn}	–1	1	–1	1	–1	1	1	–1
q_{pn}	–1	1	1	–1	–1	–1	–1	1
w_1	1	–1	1	–1	1	–1	1	–1
$w_1 i_{pn}$	–1	–1	–1	–1	–1	–1	1	1
$w_1 q_{pn}$	–1	–1	1	1	–1	1	–1	–1
d_1	1	.....			–1	.....		
$d_1 w_1 i_{pn}$	–1	–1	–1	–1	1	1	–1	–1
$d_1 w_1 q_{pn}$	–1	–1	1	1	1	–1	1	1
a_1	0.6	.....						
$I_1 = a_1 d_1 w_1 i_{pn}$	–0.6	–0.6	–0.6	–0.6	0.6	0.6	–0.6	–0.6
$Q_1 = a_1 d_1 w_1 q_{pn}$	–0.6	–0.6	0.6	0.6	0.6	–0.6	0.6	0.6

First, the i_{pn} and q_{pn} sequences are multiplied by Walsh word w_1 = (1 –1 1 –1) repeated every 4 chips. This result is then multiplied by the data sequence $d_1 = 1$ for the first 4 chips and $d_2 = –1$ for the next 4 chips, and finally, the two sequences are

multiplied by the amplitude $a_1 = 0.6$. Values of –0.6 were arbitrarily added for time t_9 to be used later to illustrate the effect of time offset. The resulting sequences for I_0,Q_0 and I_1,Q_1 are shown in Table V and their I-Q diagrams are shown in Fig. 7.

Table V
Superposition of I-Q Sequences

Time	t_1	t_2	t_3	t_4	t_5	t_6	t_7	t_8
I_0	–0.8	0.8	–0.8	0.8	–0.8	0.8	0.8	–0.8
Q_0	–0.8	0.8	0.8	–0.8	–0.8	–0.8	–0.8	0.8
I_1	–0.6	–0.6	–0.6	–0.6	0.6	0.6	–0.6	–0.6
Q_1	–0.6	–0.6	0.6	0.6	0.6	–0.6	0.6	0.6
I	–1.4	0.2	–1.4	0.2	–0.2	1.4	0.2	–1.4
Q	–1.4	0.2	1.4	–0.2	–0.2	–1.4	–0.2	1.4

In the above example, we considered the situation of a CDMA signal consisting of the pilot and code channel 1 and showed that we could obtain the I-Q diagram for the composite signal simply by superimposing the I-Q diagrams for the individual signals. For our example of two signals, the two 4-point I-Q diagrams produced an 8-point diagram for the composite signal. This principle of superposition can be applied to any number of code channels and provides a convenient geometric way of constructing and visualizing signals. For example, if we consider three code channels with signal amplitudes of a_0, a_1, and a_2, then we obtain an I-Q diagram with coordinates (x,y) in which x and y take on the eight values $\pm a_0 \pm a_1 \pm a_2$ to produce a signal constellation with 16 points. We must keep in mind that the above discussion applies only for the condition of zero intersymbol interference.

Signal Acquisition (Timing and Frequency Estimation)

To perform the measurements of the CDMA signals, it is necessary to estimate the precise carrier frequency so that the signal to be measured can be converted to baseband, that is, so it can be represented in terms of an I-Q signal trajectory as discussed above. Furthermore, it is necessary to determine the timing of the signal to be measured relative to the zero time reference of the pseudonoise sequences i_{pn} and q_{pn} which are used to spread the spectrum of the transmitter signal. The estimation of timing and carrier frequency are discussed in this section.

Suppose that the transmitter signal to be measured has an unknown frequency error $\Delta\omega$, unknown phase θ_0, and an unknown time delay τ_0, so that after down-conversion to baseband, the signal available for measurement can be represented in the form of equation 7 with ω_c replaced with $\omega_c+\Delta\omega$, t replaced with $t-\tau_0$, and a phase term θ_0 added. That is, the signal to be measured can be represented as:

$$X(t-\tau_0) = A(t-\tau_0)\cos[(\omega_c+\Delta\omega)(t-\tau_0)+\Phi(t-\tau_0)+\theta_0], \quad (18)$$

which can be written, using the trigonometric identity $\cos(\theta+\varphi) = \cos\theta\cos\varphi - \sin\theta\sin\varphi$, as:

$$X(t-\tau_0) =$$

$$A(t-\tau_0)\cos[\Delta\omega t - (\omega_c+\Delta\omega)\tau_0 + \Phi(t-\tau_0)+\theta_0]\cos\omega_c t \quad (19)$$

$$- A(t-\tau_0)\sin[\Delta\omega t - (\omega_c+\Delta\omega)\tau_0 + \Phi(t-\tau_0) + \theta_0]\sin\omega_c t.$$

From equation 19, we obtain the in-phase and quadrature components as:

$$I_x(t) = A(t-\tau_0)\cos[\Delta\omega t-(\omega_c+\Delta\omega)\tau_0+\Phi(t-\tau_0)+\theta_0] \quad (20)$$

and

$$Q_x(t) = A(t-\tau_0)\sin[\Delta\omega t-(\omega_c+\Delta\omega)\tau_0+\Phi(t-\tau_0)+\theta_0] \quad (21)$$

Using Euler's identity, $e^{j\theta} = \exp(j\theta) = \cos\theta + j\sin\theta$, we can write the complex envelope as:

$$\begin{aligned} Y(t) &= I_x(t) + jQ_x(t) \\ &= A(t-\tau_0)\exp\left\{j[\Delta\omega t-(\omega_c+\Delta\omega)\tau_0+\Phi(t-\tau_0)+\theta_0]\right\}, \end{aligned} \quad (22)$$

from which we see that the baseband signal is a rotating phasor with magnitude $A(t-\tau_0)$ and phase $[\Delta\omega t - (\omega_c+\Delta\omega)\tau_0 + \Phi(t-\tau_0) + \theta_0]$ as shown in Fig. 8.

We see that if $\tau_0 \neq 0$ but $\Delta\omega = 0$, then the amplitude $A(t-\tau_0)$ and phase $\Phi(t-\tau_0)$ are delayed versions of $A(t)$ and $\Phi(t)$ and a phase shift of $-\omega_c\tau_0+\theta_0$ is added. Therefore, the effect of the time delay is simply a rotation of the I-Q diagram by an angle of $-\omega_c\tau_0+\theta_0$ and a change of τ_0 in the times at which the signal trajectory passes through the constellation points. When

Fig. 7. *Signal constellation and trajectory for (a) pilot channel, (b) code channel 1, and (c) the sum of the pilot channel and code channel 1.*

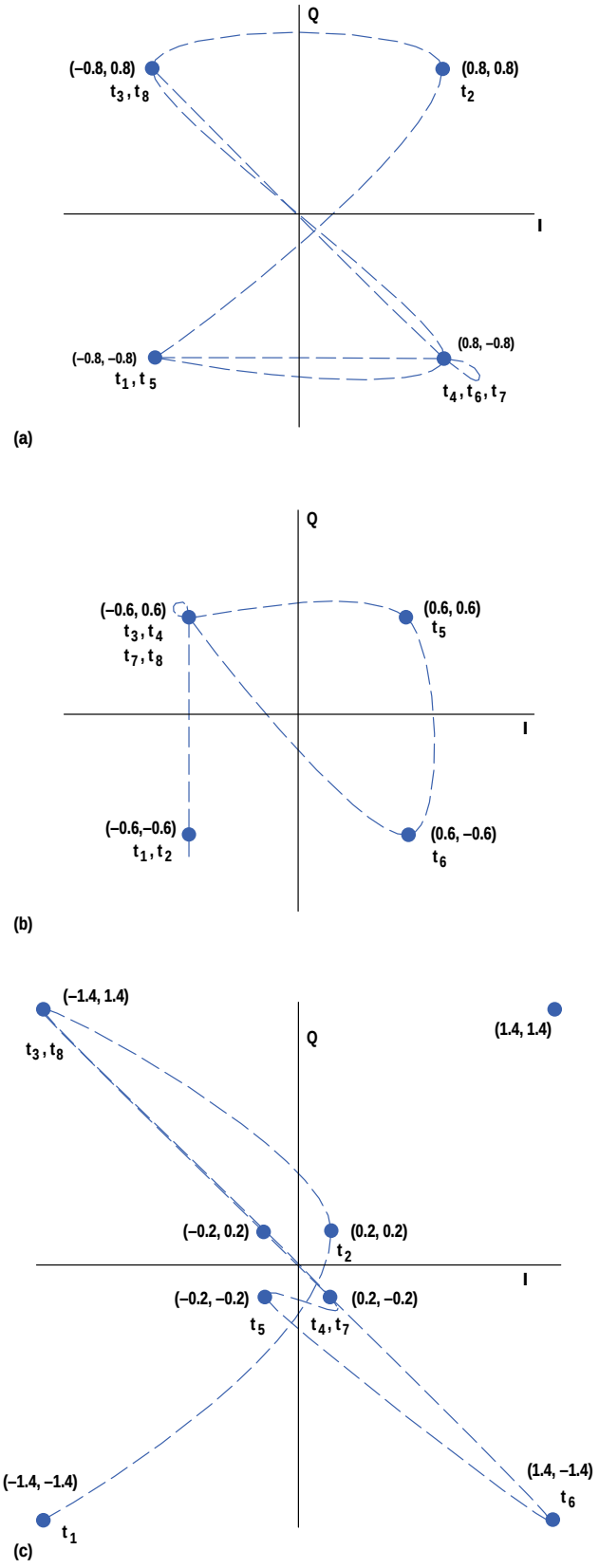

$\Delta\omega \neq 0$, the frequency error adds an additional phase shift of $-\Delta\omega\tau_0$ and a constant-rate phase rotation of $\Delta\omega t$. The result of

Fig. 8. *Complex envelope of the baseband signal.*

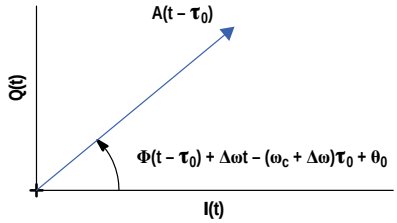

the constant-rate phase rotation will, in general, be that the signal trajectory will no longer pass through discrete points, so the I-Q diagram will not resemble its counterpart for zero frequency error.

The functions used to estimate τ_0, $\Delta\omega$, and θ_0 can be described by considering a pilot reference signal given as:

$$S(t-\tau_R, \omega_R) = A_0(t-\tau_R)\exp\left\{j\left[\omega_R t + \Phi_0(t-\tau_R)\right]\right\} , \quad (23)$$

in which $A_0(t)$ and $\Phi_0(t)$ are the instantaneous amplitude and phase of the complex envelope corresponding to the pilot only, τ_R is a variable time delay, and ω_R is a variable frequency. Using the observable baseband signal Y(t) given by equation 22 and the reference signal given by equation 23, the correlation function for these two signals is:

$$P(\tau_R, \omega_R) = \sum_k Y(t_k) S^*(t_k-\tau_R, \omega_R) . \quad (24)$$

The sample interval $t_k - t_{k-1}$ used here is different from that used previously and, in general, would be a fraction of the chip interval. The magnitude of $P(\tau_R,\omega_R)$ could be maximized with respect to τ_R and ω_R to determine the estimates $\hat{\tau}_0$ and $\Delta\hat{\omega}$ of τ_0 and $\Delta\omega$. However, a normalized version of the squared magnitude of this function is used to facilitate the search strategy for finding $\hat{\tau}_0$. $\hat{\tau}_0$ is found by forming the function

$$\frac{|P(\tau_R, 0)|^2}{\sum_k |S(t_k-\tau_R, 0)|^2 \sum_k |Y(t_k)|^2} \quad (25)$$

and finding the value $\tau_R = \hat{\tau}_0$ for which this function is maximum.

Maximizing equation 25 corresponds to maximizing the correlation between the observable baseband signal and an ideal reference signal for the pilot only. Usually, the observable baseband signal will consist of the superposition of a number of code channels. However, since the correlation between the pilot and the other code channels is small, the maximization of equation 25 provides a good initial estimate of τ_0.

$P(\tau_R, 0)$ is sensitive to frequency error $\Delta\omega$, which limits the range of $\Delta\omega$ for which equation 25 can be used. We can obtain an expression for the frequency response of $P(\tau_0,0)$ by setting

$$Y(t) = S(t-\tau_0, \Delta\omega) \quad (26)$$

to obtain

$$P(\tau_0, 0) = \sum_k A_0^2(t_k-\tau_0) e^{j\Delta\omega t_k} . \quad (27)$$

To simplify the evaluation of this expression, consider sampling at points for which the signal trajectory passes through the constellation points of the pilot, so that $A_0^2(t_k-\tau_0)$ is constant. In this case, the magnitude of $P(\tau_0,0)$ is:

$$|P(\tau_0, 0)| = \frac{\sin\left(\frac{T}{2}\Delta\omega\right)}{\sin\left(\frac{T}{2K}\Delta\omega\right)} , \quad (28)$$

where T is the length of the data record used to calculate $P(\tau_0,0)$ and K is the number of samples in the data record.

From the sketch of $P(\tau_0,0)$ in Fig. 9, we see that $P(\tau_0,0) = 0$ for $\Delta\omega = 2\pi/T$. In devising the search strategy for finding $\hat{\tau}_0$, it was assumed that frequency errors would be less than $\pm\pi/T$. Therefore, reliable estimates of τ_0 can be obtained only if

$$|\Delta\omega| < \frac{\pi}{T} . \quad (29)$$

After the value of $\hat{\tau}_0$ is determined, we obtain an estimate, $\Delta\hat{\omega}$, of $\Delta\omega$ from the discriminator formed as the ratio of the difference over the sum of $|P(\hat{\tau}_0, \Delta\omega_0)|$ and $|P(\hat{\tau}_0, -\Delta\omega_0)|$:

$$\Delta\hat{\omega} = \frac{\pi}{T}\frac{|P(\hat{\tau}_0, \Delta\omega_0)| - |P(\hat{\tau}_0, -\Delta\omega_0)|}{|P(\hat{\tau}_0, \Delta\omega_0)| + |P(\hat{\tau}_0, -\Delta\omega_0)|}, \qquad (30)$$

where $\Delta\omega_0 = \pi/T$. The formation of this discriminator is illustrated in Fig. 10, where $P(\hat{\tau}_0, \Delta\omega_0)$ is shown by the upper dashed curve, $-P(\hat{\tau}_0, -\Delta\omega_0)$ is shown by the lower dashed curve, and the discriminator curve, $\Delta\hat{\omega}T/\pi$, is shown by the solid curve.

Fig. 9. *The correlation function $P(\tau_0,0)$ as a function of frequency error.*

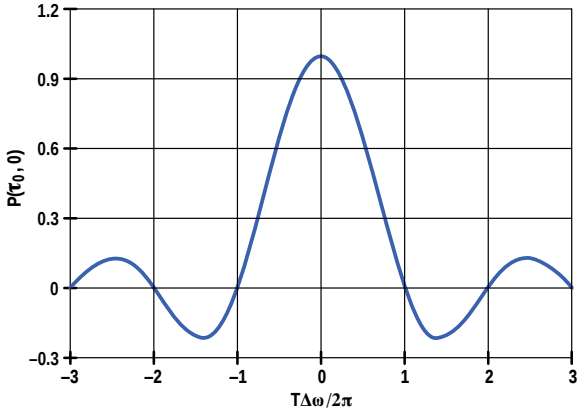

The function given by equation 30 is a linear function of $\Delta\omega$ for $|\Delta\omega| < \pi/T$ and provides a reasonably good initial estimate of the frequency error when a significant percentage (on the order of 10% or more) of the total transmitter power is contained in the pilot channel.

An estimate of the transmitter phase is obtained from the phase of the correlation function with $\tau_R = \hat{\tau}_0$ and $\omega_R = \Delta\hat{\omega}$:

$$\hat{\theta}_0 = \tan^{-1}\left[\frac{\Im\{P(\hat{\tau}_0, \Delta\hat{\omega})\}}{\Re\{P(\hat{\tau}_0, \Delta\hat{\omega})\}}\right] \qquad (31)$$

where $\Re\{z\}$ and $\Im\{z\}$ are the real and imaginary parts of z, respectively.

Fig. 10. *Formation of the discriminator of equation 30. $P(\hat{\tau}_0, \Delta\omega_0)$ is shown by the upper dashed curve, $-P(\hat{\tau}_0, -\Delta\omega_0)$ is shown by the lower dashed curve, and the discriminator curve, $\Delta\hat{\omega}T/\pi$, is shown by the solid curve.*

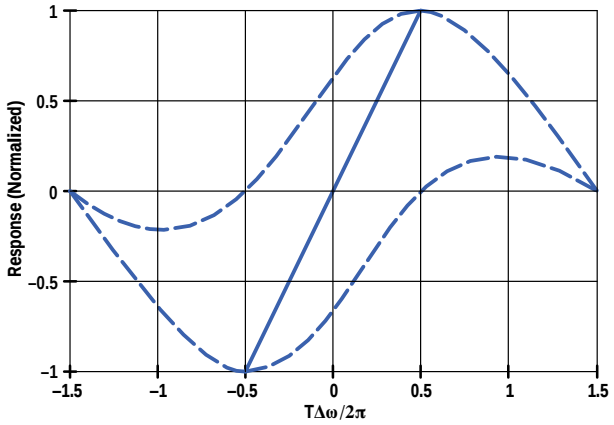

Because of the weak correlation between the pilot channel and the other code channels, equations 25, 30, and 31 provide good initial estimates of τ_0, $\Delta\omega$, and θ_0. The estimates of these parameters are refined after the intersymbol interference has been removed by the complementary filter discussed later in this article. Further refinement of these parameters is achieved when estimating time and phase offsets of the code channels relative to the pilot channel. The estimation of the offset parameters is discussed later in this article.

Code-Domain Power Spectrum

The code-domain power spectrum is given in terms of the coefficients ρ_i, where ρ_i is defined as the fractional part of the transmitter power contained in the ith code channel. The first step in calculating the code-domain power spectrum is to multiply $I(t_k)$ and $Q(t_k)$ by i_{pn} and q_{pn}. The results of these calculations are shown in Table VI.

Table VI
Despreading of I_k and Q_k

	1st Walsh function interval				2nd Walsh function interval			
Time	t_1	t_2	t_3	t_4	t_5	t_6	t_7	t_8
$I(t_k)$	–1.4	0.2	–1.4	0.2	–0.2	1.4	0.2	–1.4
$Q(t_k)$	–1.4	0.2	1.4	–0.2	–0.2	–1.4	–0.2	1.4
i_{pn}	–1	1	–1	1	–1	1	1	–1
q_{pn}	–1	1	1	–1	–1	–1	–1	1
$Z_I = I \cdot i_{pn}$	1.4	0.2	1.4	0.2	0.2	1.4	0.2	1.4
$Z_Q = Q \cdot q_{pn}$	1.4	0.2	1.4	0.2	0.2	1.4	0.2	1.4

The code-domain power spectrum is:

$$\rho_i = \frac{1}{\sum_{k=1}^{M} |R_{ik}|^2} \quad \frac{\sum_{h=1}^{N} \left| \sum_{k=1}^{M} Z_{hk} R_{ik}^* \right|^2}{\sum_{h=1}^{N} \sum_{k=1}^{M} |Z_{hk}|^2}, \qquad (32)$$

where Z_{hk} is the kth sample of the despread signal in the hth Walsh function interval, R_{ik} is the kth chip of the ith Walsh function, M is the number of chips in a Walsh function, and N is the number of Walsh function intervals in the measurement interval. The calculations of ρ_i, i = 0, 1, 2, 3 for the above example are presented in Table VII ($j = \sqrt{-1}$).

Table VII
Calculation of ρ_i for the Example

	Z_{hk}	R_{0k}	$Z_{hk}R^*_{0k}$	R_{1k}	$Z_{hk}R^*_{1k}$
h=1	1.4+j1.4	1+j	2.8	1+j	2.8
”	0.2+j0.2	1+j	0.4	–1–j	–0.4
”	1.4+j1.4	1+j	2.8	1+j	2.8
”	0.2+j0.2	1+j	0.4	–1–j	–0.4
h=2	0.2+j0.2	1+j	0.4	1+j	0.4
”	1.4+j1.4	1+j	2.8	–1–j	–2.8
”	0.2+j0.2	1+j	0.4	1+j	0.4
”	1.4+j1.4	1+j	2.8	–1–j	–2.8

$$\sum_{k=1}^{4} |R_{ik}|^2 = 8$$

$$\sum_{h=1}^{2} \sum_{k=1}^{4} |Z_{hk}|^2 = 8\left(1.4^2\right) + 8\left(0.2^2\right) = 16 \qquad (33)$$

$$\sum_{h=1}^{2} \left| \sum_{k=1}^{4} Z_{hk} R_{0k} \right|^2 = 6.4^2 + 6.4^2 = 81.92 \qquad (34)$$

$$\rho_0 = \frac{81.92}{8(16)} = \frac{81.92}{128} = 0.64 \qquad (35)$$

$$\sum_{h=1}^{2} \left| \sum_{k=1}^{4} Z_{hk} R_{1k} \right|^2 = 4.8^2 + 4.8^2 = 46.08 \qquad (36)$$

$$\rho_1 = \frac{46.08}{128} = 0.36 \qquad (37)$$

$$\rho_2 = \rho_3 = 0 \qquad (38)$$

$$\rho_0 + \rho_1 + \rho_2 + \rho_3 = 1.0000\ . \qquad (39)$$

Since we selected signal amplitudes $a_0 = 0.8$ and $a_1 = 0.6$, the total signal energy in our measurement interval (two Walsh function intervals) is proportional to $(0.8^2 + 0.6^2) = 1.0$ and the percentages of signal energy in the pilot and code channel 1, respectively, are $0.8^2 = 0.64$ and $0.6^2 = 0.36$. We see, therefore, that the results of this example verify that ρ_i is the fractional part of the energy of the observed signal that is contained in the ith code channel.

Errors

Various errors will produce a transmitter signal that does not match the ideal reference signal. These errors will manifest themselves as a distribution of the transmitter signal energy among the code channels that varies from the ideal distribution. As mentioned earlier, the transmitter signal may have an unknown time reference and carrier frequency. However, as we saw, these parameters are estimated so that they can be removed from the signal to be measured. Therefore, frequency errors and time delay are compensated to a sufficient degree of accuracy to have minimal influence on the distribution of code-domain power.

Other types of errors are not compensated. These include signal impairments caused by nonideal components in the transmitter such as nonideal filters, nonlinearities, gain and phase imbalances, mixer spurs, quantization errors, and others.

Waveform Quality Factor (ρ). A measure of the quality of the transmitter signal is obtained by measuring ρ, defined as:

$$\rho = \frac{\left|\sum_k Z_k R_{0k}^*\right|^2}{\sum_k |R_{0k}|^2 \sum_k |Z_k|^2} \qquad (40)$$

where Z_k is the kth sample of the despread signal, $R^*_{0k} = 1–j$, and only the pilot is transmitted. By comparing equations 40 and 32, we see that ρ and ρ_0 are similar but not identical. When ρ_0 is calculated, the energy in code channel 0 is found for each Walsh function interval in the measurement interval and the sum of these energies is obtained. When ρ is calculated, the energy of the projection onto $R^*_{0k} = 1–j$ over the entire measurement interval is obtained. For random type errors, values obtained for ρ and ρ_0 will be essentially equal. However, certain types of errors such as uncompensated frequency errors will yield different values for ρ and ρ_0.

According to equations 32 and 40, a fixed phase difference between the measured baseband signal and the reference signal will not affect ρ and ρ_i. This is true because these functions involve the calculation of energies that are insensitive to phase, that is,

$$\left|e^{j\theta_0}\ ZR^*\right|^2 = \left|ZR^*\right|^2.$$

Time and Phase Offset Errors. Time offsets and phase offsets of the code channels relative to the pilot channel are errors with tolerances specified in IS-97. Offset errors in a particular code channel will cause energy from that code channel to leak into other code channels and thereby cause a change in the distribution of code-domain power. An example of time and phase offset errors is considered in this section.

Suppose there are time and phase offsets of channel 1 with respect to channel 0 of $\Delta\tau_1$ and $\Delta\theta_1$, respectively. For illustrative purposes, we will assume that the pulse response of the transmit filter is triangular, as shown in Fig. 11, so the transmit filter is considered a linear interpolator of adjacent input values. We will extend our example by considering the effects of offsets of $\Delta\tau_1 = 0.1/T_c$, where T_c is the chip interval, and $\Delta\theta_1 = 0.1$ radian. We compute I_1 and Q_1 for this case as presented in Table VIII.

Table VIII
Calculation of ρ_i for the Example with Time and Phase Offsets

From timing error (linearly interpolate 90% current value, 10% future value)

Time	t_1	t_2	t_3	t_4	t_5	t_6	t_7	t_8
I_1	–0.6	–0.6	–0.6	–0.48	0.6	0.48	–0.6	–0.6
Q_1	–0.6	–0.48	0.6	0.6	0.48	–0.48	0.6	0.48

From phase error ($I_1\cos0.1 - Q_1\sin0.1$, $I_1\sin0.1 + Q_1\cos0.1$)

I_1	–0.5371	–0.5491	–0.6569	–0.5375	0.5491	0.5255	–0.6569	–0.6449
Q_1	–0.6569	–0.5375	0.5371	0.5491	0.5375	–0.4297	0.5371	0.4177
I_0	–0.8	0.8	–0.8	0.8	–0.8	0.8	0.8	–0.8
Q_0	–0.8	0.8	0.8	–0.8	–0.8	–0.8	–0.8	0.8
I	–1.3371	0.2509	–1.4569	0.2625	–0.2509	1.3255	0.1431	–1.4449
Q	–1.4569	0.2625	1.3371	–0.2509	–0.2625	–1.2297	–0.2629	1.2177

Multiply by i_{pn} and q_{pn} to obtain $Z = Z_I + jZ_Q$

Z_I	1.3371	0.2509	1.4569	0.2625	0.2509	1.3255	0.1431	1.4449
Z_Q	1.4569	0.2625	1.3371	0.2509	0.2625	1.2297	0.2629	1.2177

	Z_{hk}	R_{0k}	$Z_{hk}R^*_{0k}$	R_{1k}	$Z_{hk}R^*_{1k}$
h=1	1.3371+j1.4569	1+j	2.7940+j0.1198	1+j	2.7940+j0.1198
”	0.2509+j0.2625	1+j	0.5134+j0.0116	–1–j	–0.5134–j0.0116
”	1.4569+j1.3371	1+j	2.7940–j0.1198	1+j	2.7940–j0.1198
”	0.2625+j0.2509	1+j	0.5134–j0.0116	–1–j	–0.5134+j0.0116
h=2	0.2509+j0.2625	1+j	0.5134+j0.0116	1+j	0.5134+j0.0116
”	1.3255+j1.2297	1+j	2.5552–j0.0958	–1–j	–2.5552+j0.0958
”	0.1431+j0.2629	1+j	0.4060+j0.1198	1+j	0.4060+j0.1198
”	1.4449+j1.2177	1+j	2.6626–j0.2272	–1–j	–2.6626+j0.2272

	Z_{hk}	R_{2k}	$Z_{hk}R^*_{2k}$	R_{3k}	$Z_{hk}R^*_{3k}$
h=1	1.3371+j1.4569	1+j	2.7940+j0.1198	1+j	2.7940+j0.1198
”	0.2509+j0.2625	1+j	0.5134+j0.0116	–1–j	–0.5134–j0.0116
”	1.4569+j1.3371	–1–j	–2.7940+j0.1198	–1–j	–2.7940+j0.1198
”	0.2625+j0.2509	–1–j	–0.5134+j0.0116	1+j	0.5134–j0.0116
h=2	0.2509+j0.2625	1+j	0.5134+j0.0116	1+j	0.5134+j0.0116
”	1.3255+j1.2297	1+j	2.5552–j0.0958	–1–j	–2.5552+j0.0958
”	0.1431+j0.2629	–1–j	–0.4060–j0.1198	–1–j	–0.4060–j0.1198
”	1.4449+j1.2177	–1–j	–2.6626+j0.2272	1+j	2.6626–j0.2272

From the values obtained in Table VIII, we compute the code-domain power coefficients as follows:

$$\sum_{k=1}^{4}|R_{ik}|^2\sum_{h=1}^{2}\sum_{k=1}^{4}|Z_{hk}|^2 = 121.1648\ . \tag{41}$$

$$\sum_{h=1}^{2}\left|\sum_{k=1}^{4}Z_{hk}R_{0k}^{*}\right|^2 = |6.6148|^2 + |6.1372-j0.1916|^2 = 81.4575\ . \tag{42}$$

$$\sum_{h=1}^{2}\left|\sum_{k=1}^{4}Z_{hk}R_{1k}^{*}\right|^2 = |4.5612|^2 + |-4.2984+j0.4544|^2 = 39.4873\ . \tag{43}$$

$$\sum_{h=1}^{2}\left|\sum_{k=1}^{4}Z_{hk}R_{2k}^{*}\right|^2 = |j0.2628|^2 + |j0.0232|^2 = 0.0696\ . \tag{44}$$

$$\sum_{h=1}^{2}\left|\sum_{k=1}^{4}Z_{hk}R_{3k}^{*}\right|^2 = |0.2164|^2 + |0.2148-j0.2396|^2 = 0.1504\ . \tag{45}$$

$$\rho_0 = \frac{81.4575}{121.1648} = 0.6723 \tag{46}$$

$$\rho_1 = \frac{39.4873}{121.1648} = 0.3259 \tag{47}$$

$$\rho_2 = \frac{0.0696}{121.1648} = 0.0006 \tag{48}$$

$$\rho_3 = \frac{0.1504}{121.1648} = 0.0012 \tag{49}$$

We note that the timing and phase errors caused some of the energy from code channel 1 to leak into the other code channels. However, again

$$\rho_0 + \rho_1 + \rho_2 + \rho_3 = 1.0000\ . \tag{50}$$

This condition is always satisfied regardless of the errors introduced to the data sequence $Z = Z_I + jZ_Q$.

Estimates of Time and Phase Offsets. We saw in the above example that when code channel 1 was offset in time and phase relative to the pilot channel, errors were introduced that caused the relative energy to increase in code channels 0, 2, and 3 and to decrease in channel 1. To determine the values of the offset errors, the mean squared difference between the observable data, Z, and an ideal reference signal, R, is minimized. For the example considered above, the errors introduced by timing and phase offsets are equal to the difference in $Z_I + jZ_Q$ for the case of no errors given in Table VII and the case with phase and time offset errors given in Table VIII. These errors as a function of time t_k are listed in Table IX.

Fig. 11. *Simplified impulse response of the transmit filter.*

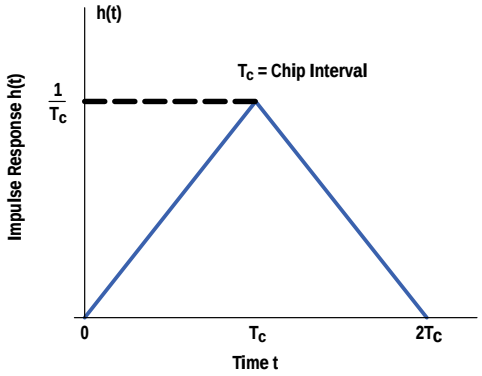

Using the listed values, the mean squared error is:

$$\begin{aligned} MSE &= \frac{1}{8}\sum_{k=1}^{8}\left|E_{Qk} + jE_{Ik}\right|^2 \\ &= \frac{1}{8}\sum_{k=1}^{8}\left(E_{Qk}^2 + E_{Ik}^2\right) \\ &= 0.13876. \end{aligned} \tag{51}$$

To estimate timing and phase offset errors, the active code channels are determined by calculating ρ_i for every i and identifying the channels for which the values of ρ_i are above a preset threshold. For example, if a threshold of 0.01 (corresponding to –20 dB) is used, every channel for which $\rho_i > 0.01$ will be declared an active channel.

In addition to determining the active code channels, it is necessary to determine the data sequence d_{ih} for each active channel in which the subscript i denotes the ith code channel and the subscript h denotes the hth Walsh function interval in the measurement interval. The data detector incorporated into the function used to calculate ρ_i is:

$$\hat{d}_{ih} = \operatorname{sgn}\left(\Re\left\{\sum_k Z_{hk}R_{ik}^*\right\}\right), \tag{52}$$

where

$$\begin{aligned} \operatorname{sgn}(u) &= \;\;1, \quad u > 0 \\ &= -1, \quad u < 0 \end{aligned} \tag{53}$$

and $\Re\{z\}$ is the real part of z. The index k varies over the chips in a Walsh function interval (k = 0 to 3 in our example). From the values tabulated in Table VIII, we can generate the detected data as shown in Table X.

Table IX
In-Phase (E_I) and Quadrature (E_Q) Components of Errors in Example for Timing and Phase Offset Errors

Time	t_1	t_2	t_3	t_4	t_5	t_6	t_7	t_8
E_I	–0.0629	0.0509	0.0569	0.0625	0.0509	–0.0745	–0.0569	0.0449
E_Q	0.0569	0.0625	–0.0629	0.0509	0.0625	–0.1703	0.0629	–0.1823

Table X
Calculations for Data Detection in the Example

i,h	ρ_i	$\sum_{k=1}^{4} Z_{hk}R_{0k}^*$	$\hat{d}_{ih}$
0,1	0.6723 (active)	6.6148	1
0,2	”	6.1372	1
1,1	0.3259 (active)	4.5612	1
1,2	”	–4.2984+j0.4544	–1
2,1	0.0006 (inactive)		
2,2	”		
3,1	0.0012 (inactive)		
3,2	”		

After the active code channels and their data sequences are determined, an ideal signal of the form of equations 9 and 10 can be generated for each active code channel. The in-phase and quadrature components of the ideal signals are:

$$I_i(t) = A_i(t)\cos\Phi_i(t) \tag{54}$$

and

$$Q_i(t) = A_i(t)\sin\Phi_i(t) \tag{55}$$

where $A_i(t)$ and $\Phi_i(t)$ are the amplitude and phase of the ideal signal of the ith code channel passing through the points (±1,±1) in the I-Q diagram as shown in Fig. 6. The reference signal is generated by superimposing the ideal signals given by equations 54 and 55 for each active code channel. The resulting in-phase and quadrature components of the ideal reference signal are:

$$I_{ref}(t) = \sum_i \hat{\alpha}_i A_i(t-\hat{\tau}_i)\cos\left[\Delta\hat{\omega}t + \Phi_i(t-\hat{\tau}_i) + \hat{\theta}_i\right] \quad (56)$$

and

$$Q_{ref}(t) = \sum_i \hat{\alpha}_i A_i(t-\hat{\tau}_i)\sin\left[\Delta\hat{\omega}t + \Phi_i(t-\hat{\tau}_i) + \hat{\theta}_i\right], \quad (57)$$

where $\Delta\hat{\omega}$ is frequency error, $\hat{\alpha}_i$ is the relative amplitude $\left(\hat{\alpha}_i \approx \sqrt{\rho_i}\right)$, $\hat{\tau}_i$ is the time delay, and $\hat{\theta}_i$ is the phase of the ith code channel. The summations are over the set of active code channels.

The frequency error, time delays, and phases are determined by finding values of $\Delta\hat{\omega}$, $\hat{\alpha}_i$, $\hat{\tau}_i$, and $\hat{\theta}_i$ for all values of i corresponding to the active code channels to minimize the mean squared difference between the observable sequence $Z(t_k) = Z_I(t_k) + jZ_Q(t_k)$ and the reference $R(t_k) = I_{ref}(t_k) + jQ_{ref}(t_k)$, which is:

$$\overline{\epsilon^2} = \frac{1}{NM}\sum_{k=1}^{NM}\left|Z(t_k) - R(t_k)\right|^2, \quad (58)$$

where M and N are the same as in equation 32. $\hat{\tau}_0$ and $\Delta\hat{\omega}$ are used to update previous estimates of time delay and frequency. Estimates of time and phase offsets obtained from $\hat{\tau}_i$ and $\hat{\theta}_i$ are:

$$\Delta\hat{\tau}_i = \hat{\tau}_i - \hat{\tau}_0$$

and (59)

$$\Delta\hat{\theta}_i = \hat{\theta}_i - \hat{\theta}_0.$$

For the example above, values of $\Delta\hat{\omega}$, $\hat{\alpha}_i$, $\hat{\tau}_i$, and $\hat{\theta}_i$ would be found to produce zero mean squared difference and error-free estimates of these parameters. In general, however, errors other than those introduced by timing and phase offsets would be present, so that after the minimization of the mean squared difference, a nonzero residual between the reference and the observable would exist and the parameters would be estimated with some error in the estimates.

Signal Flow Diagram

The signal flow diagram for the CDMA power, timing, and phase offset measurement algorithms is shown in Fig. 12. The signal under test from the base station transmitter is down-converted to a 3.6864-MHz IF signal that is sampled at 4.9152 MSa/s. The digitized IF signal is passed through a finite-impulse-response (FIR), linear-phase, digital IF filter centered at 1.2288 MHz. This filter has a flat passband 1.4 MHz wide, which is considerably wider than the 1.23-MHz bandwidth of the IF signal and provides blocking at dc and 359.2 kHz. Indeed, the primary purpose of the IF filter is to block these signal components.

Following the IF filter, the signal is down-converted to in-phase (I) and quadrature (Q) baseband signals. In the down-converter, the I and Q signals are filtered by flat, FIR, linear-phase, low-pass filters with passbands from 0 to 700 kHz wide and stop bands from 1.16 to 2.0 MHz wide. The full sample rate of 4.9152 MSa/s is retained at the output of the down-converter to provide maximum accuracy at the correlator.

The next function after the down-converter is the correlator, which provides an estimate of the timing of the signal under test. The inputs to the correlator are the baseband signal from the down-converter and an internally generated reference signal. This reference signal is the mathematically ideal signal that would be present at the output of the down-converter if only the pilot signal were transmitted. The time origin of the reference signal corresponds to the first binary 1 following 15 binary 0s of the pseudonoise sequences i_{pn} and q_{pn}, as specified in the IS-95 standard.

The correlator performs the timing acquisition described earlier by finding the value of τ_R that maximizes the function given by expression 25. Since this function is sensitive to frequency error, the correlator works reliably over a limited range of frequency. If T is the length of the record (in seconds) used in the correlator, then the maximum frequency error for which the correlator will provide reliable acquisition is:

$$\Delta f_{max} = \frac{1}{2T}. \quad (60)$$

For example, if a 1.25-ms time record is used, then the maximum frequency error that will allow reliable acquisition in time is $\pm\Delta f_{max} = \pm 400$Hz.

Fig. 12. *Signal flow diagram for the HP 83203B CDMA power, timing, and phase offset measurement algorithms.*

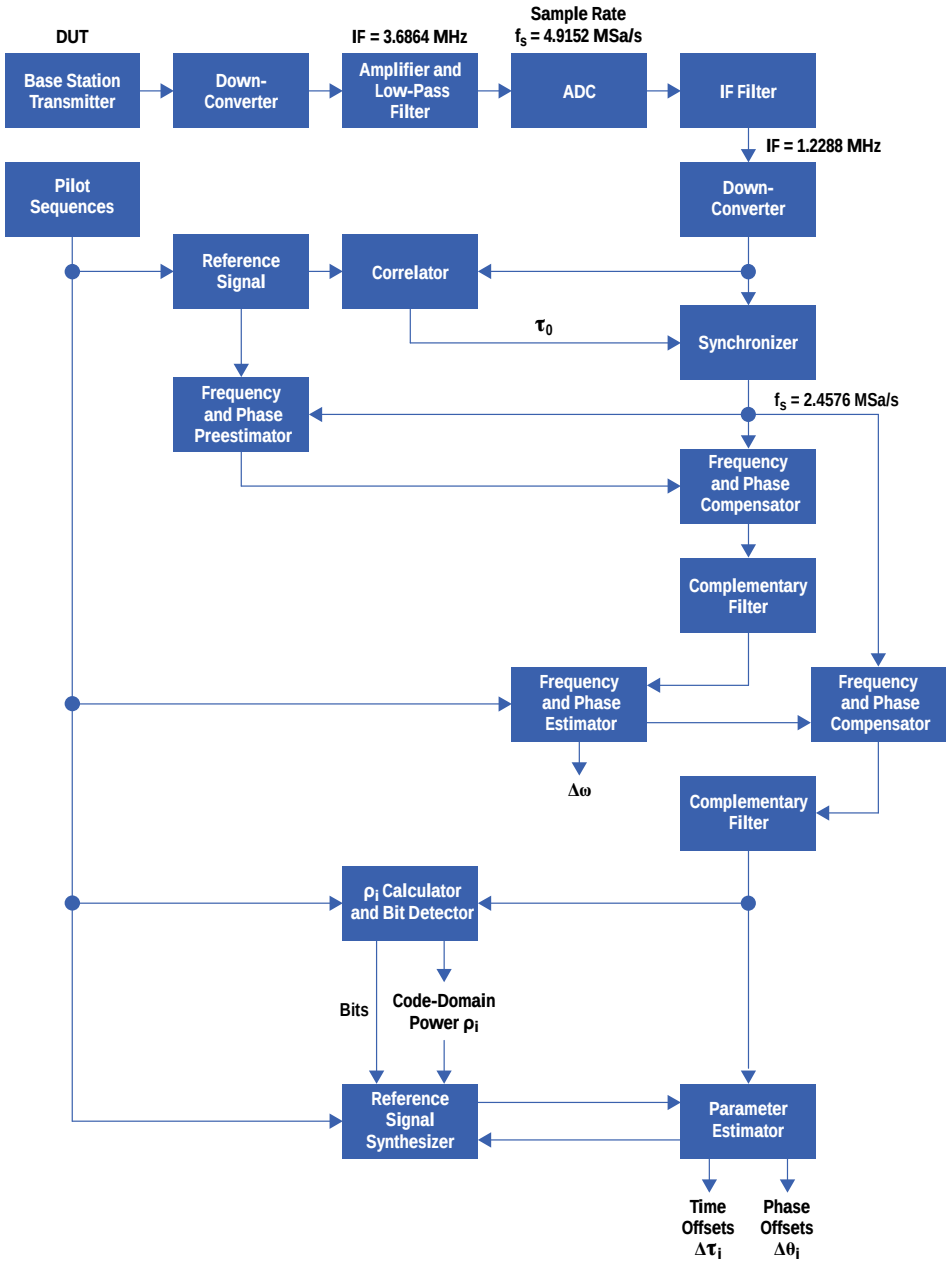

After the time delay τ_0 is determined, the baseband signal is time-aligned with the reference signal. This function is performed in the synchronizer, which consists of a pair (for I and Q) of low-pass filters that resample the signals at a rate of 2.4576 MSa/s with a variable time delay to introduce the appropriate timing.

The synchronized baseband and reference signals are used in the frequency and phase preestimator to obtain initial estimates of the carrier frequency and phase as given by equations 30 and 31. These estimates are then used in the frequency and phase compensator to largely remove $\Delta\omega$ and θ_0 from the baseband signals.

After obtaining a baseband signal that is compensated in frequency and phase, the next step is to remove the intersymbol interference introduced by the transmit filter. This step is necessary to ensure the orthogonality of the code channels to allow calculation of the code-domain power coefficients by the algorithm discussed earlier. Intersymbol interference is removed by the complementary filter, which when cascaded with the transmit filter produces an overall filter response that satisfies Nyquist's criterion for zero intersymbol interference.

After the intersymbol interference is removed from the baseband signal by the complementary filter, refined estimates of the carrier frequency and phase are obtained by minimizing the mean squared difference between the baseband signal and a reference signal consisting of only the pilot. The procedure used here is similar to that used for estimating the frequency and phase in conjunction with the time and phase offsets as described earlier. After the intersymbol interference has been

removed, it is unnecessary to include the effect of the transmit filters; this allows the pilot sequences to be used directly as the reference signals.

After the refined estimates of carrier frequency and phase are obtained, the baseband signal is again passed through a compensator and a complementary filter to improve the removal of frequency error, phase error, and intersymbol interference from the baseband signal.

Following this second stage of compensation, the baseband signal is ready to be used for calculating ρ_i as described earlier. This function is performed in the ρ_i calculator shown in the signal flow diagram. Data bits are also detected in this function that are needed to calculate the reference signal used for estimating time and phase offsets of code channels as described earlier. This function could also be used to calculate the waveform quality factor ρ. However, this parameter is actually calculated by another function developed for the HP 83203A using the procedure given in an earlier section.

The final steps in the signal flow diagram involve determining the time offsets and phase offsets of the active code channels relative to the pilot channel. To estimate these offset parameters, it is necessary to generate an ideal reference signal corresponding to the active code channels in which the amplitudes, phases, time delays, and frequencies of all of the code channels in the reference signal can be controlled. The function that generates this ideal reference signal, referred to as the *reference signal synthesizer*, is invoked by the parameter estimator, which uses a search procedure to minimize the mean squared difference between the baseband test signal and the synthesized reference signal as described earlier.

Accuracy of the Measurement Equipment

Specifications for the HP 83203B (HP 8921A/600) are warranted performance. These specifications are derived from the accuracy of the measurement algorithms, environmental considerations, measurement uncertainties, unit-to-unit variations, and customer specification margins. Typical performance of the HP 83203B is significantly better than the published specifications.

The minimum performance of a base station transmitter is specified in the IS-97 standard. In section 11.1.3 of this standard, Table 11.1.3.1, reproduced here as Table XI, specifies the frequency tolerance, time reference, pilot waveform quality, and RF power output variation.

Table XI
Environmental Test Limits
(from Table 11.1.3-1 in IS-97 Standard)

Parameter	Limit
Frequency Tolerance	± 0.05 ppm
Time Reference	± 10 μs
Pilot Waveform Quality	$\rho > 0.912$
RF Power Output Variation	+2 dB, −4 dB

The carrier frequency of the RF signal to be tested is approximately 900 MHz, so the frequency tolerance given above corresponds to an absolute frequency tolerance of ±45 Hz. Since the HP 83203B can acquire a signal and accurately estimate the frequency error when the frequency error is as large as ±400 Hz for a 1.25-ms measurement interval, frequency errors within the above tolerance are easily accommodated.

The tolerance on pilot waveform quality significantly impacts the accuracy of the measurement algorithms. Error-vector-magnitude-squared (evm^2), which is defined as the ratio of the energy of the error to the energy of the error-free transmit signal, can be shown to be approximately related to the waveform quality factor, ρ , as:

$$evm \approx \sqrt{\frac{1}{\rho} - 1}\,. \qquad (61)$$

For the value of $\rho = 0.912$ in Table XI,

$$evm \approx \sqrt{\frac{1}{0.912} - 1} = 0.31, \qquad (62)$$

that is, the waveform quality specified in Table XI corresponds to a signal with an rms error of approximately 31%.

Other errors that impact the accuracy of the measurement equipment are time errors and phase differences between the pilot channel and other code channels. Tolerances on these errors are given in sections 10.3.1.2.3 and 10.3.1.3.3 of the IS-97 standard as less than ±50 ns for time errors and less than ±50 mrad for the phase differences.

The accuracy of the waveform quality measurement equipment is specified in Table 12.4.2.1-1 of the IS-97 standard, repeated here as Table XII.

Waveform quality is measured when only the pilot is transmitted. We will discuss the accuracy in measuring each of the parameters listed above and the measurement interval necessary to achieve the performance specified.

To measure code-domain power, test models for the base station are specified in Table 12.5.2-1 of the IS-97 standard, reproduced here as Table XIII.

Table XII
Accuracy of Waveform Quality Measurement Equipment
(from Table 12.4.2.1-1 in the IS-97 Standard)

Parameter	Symbol	Accuracy Requirement
Waveform Quality	ρ	$\pm 5 \times 10^{-4}$ from 0.9 to 1.0
Frequency Error (exclusive of test equipment time-base errors)	Δf	± 10 Hz
Pilot Time Alignment	τ_0	± 135 ns

Table XIII
Base Station Test Model, Nominal
(from Table 12.5.2-1 in the IS-97 Standard)

Type	Number of Channels	Fraction of Power (linear)	Fraction of Power (dB)	Comments
Pilot	1	0.2000	–7.0	Code channel 0
Sync	1	0.0471	–13.3	Code channel 32, always 1/8-rate
Paging	1	0.1882	–7.3	Code channel 1, full-rate only
Traffic	6	0.09412	–10	Variable code channel assignments; full-rate only

The measurement algorithms have been tested and found to provide accurate results for signals with less than 10% of the power in the pilot channel; however, in discussing the accuracy of the measurement algorithms in the next subsection, we will only consider performance under the conditions prescribed by the nominal test model.

The accuracy required of the code-domain measurement equipment is given in Table 12.4.2.2-1 of the IS-97 standard using the nominal test model given above. This table is reproduced here as Table XIV.

We will discuss the accuracy of measuring each of the parameters given in Table XIV and give the minimum measurement intervals and number of subestimates that must be averaged to achieve the accuracies specified.

Accuracy of the Measurement Algorithms

Dynamic Range. The flatness of the filters and the numerical accuracy of the computations used in all of the signal processing algorithms for the HP 83203B are closely maintained to produce a computational error level of approximately –55 dB. Since this error level is typically less than the level of the spurious signals and quantization noise introduced by the analog down-conversion process and the analog-to-digital converter (ADC) used to digitize the IF signal under test, the dynamic range of the HP 83203B is limited by the noise and spurious signal level at the output of the ADC. The ADC uses autoranging to maintain the signal level at the input of the quantizer at –1 dB to –10 dB from saturation. With the ADC operating at –10 dB below saturation, the noise and

spurious signal level at the output of the ADC is approximately –45 dB relative to the digitized IF signal. Therefore, the analog and ADC hardware places a limit on the dynamic range of the code-domain power measurements of approximately 45 dB.

Table XIV
Accuracy of Code-Domain Measurement Equipment
(from Table 12.4.2.2-1 in the IS-97 Standard)

Parameter	Symbol	Accuracy Requirement
Code-domain power coefficients	ρ_i	$\pm 5 \times 10^{-4}$f rom 5×10^{-4} to 1.0
Frequency Error (exclusive of test equipment time-base errors)	Δf	±10 Hz
Code-domain time offset relative to pilot	$\Delta\tau_i$	±10 ns
Code-domain phase offset relative to pilot	$\Delta\theta_i$	±0.01 radian

Accuracy in Measuring ρ and ρ_i. The accuracy in measuring waveform quality ρ and code-domain power ρ_i depends on the accuracy of estimating time delay τ_0 and frequency error $\Delta\omega$. The errors in the measurement of ρ produced by errors in estimating τ_0 and $\Delta\omega$ are shown in Figs. 13a and 13b for measurement intervals of 1.04 ms and 2.08 ms. The error curves correspond to transmitting an ideal pilot channel for which the true value of ρ is 1.0. Since the percentage error in the measurement of ρ caused by frequency and timing errors is independent of the true value of ρ, the error curves presented here apply to values of ρ from ρ = 1.0 to ρ<0.1. From Table XII, we see that the required measurement accuracy specified in the IS-97 standard is $\pm 5 \times 10^{-4}$ for ρ = 0.9 to 1.0. This tolerance corresponds to a measurement error of −33 dB for ρ = 1.0, which is shown in Figs. 13a and 13b.

Fig. 13. *Errors in the measurement of signal quality produced by errors in estimating (a)* t_0 *and (b)* Dw *for measurement intervals of 1.04 ms and 2.08 ms. The error curves correspond to transmitting an ideal pilot channel for which the true value of* r *is 1.0 and are valid for* r = *0.1 to* r = *1.0.*

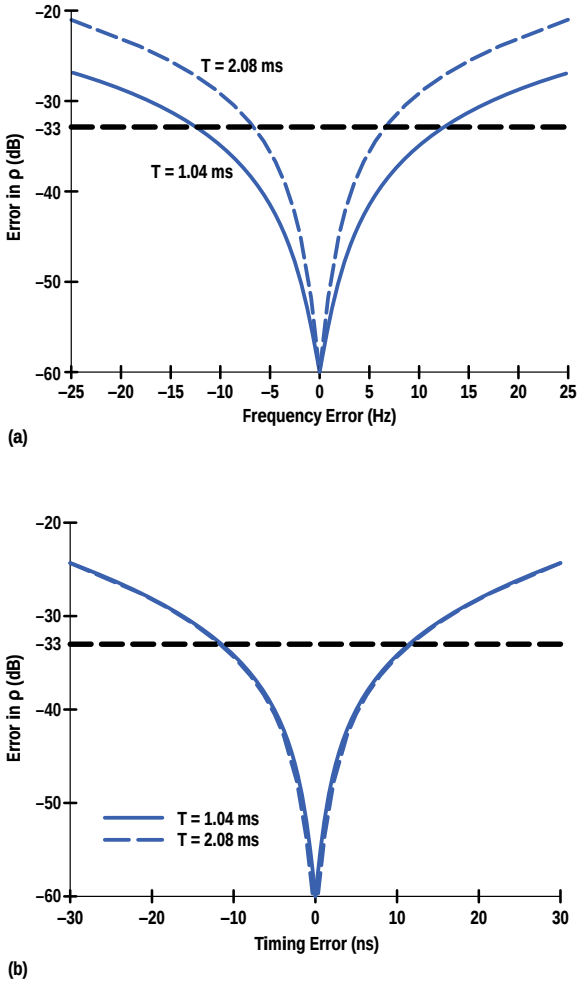

According to Table XII, frequency error must be measured to an accuracy of ±10 Hz and pilot time alignment must be measured to an accuracy of ±135 ns. The uncertainty in the time reference of the ADC and errors of the time-delay estimator

contribute to the measurement errors of pilot time delay. In the HP 83203B, the ADC will contribute less than ±125 ns error and the time-delay estimator will contribute less than ±10 ns error to the pilot time alignment measurement. Therefore, for purposes of determining the accuracies in measuring ρ and ρ_i, we can assume that limits on the errors of the measurements of τ_0 and $\Delta\omega$ are:

$$-10 \text{ ns} \leq \hat{\tau}_0 - \tau_0 \leq 10 \text{ ns}$$

and (63)

$$-10 \text{ Hz} \leq \Delta\hat{\omega} - \Delta\omega \leq 10 \text{ Hz}.$$

From the error curves in Fig. 13, we see that if the tolerances given by equation 63 are achieved, then for a measurement interval of 1.04 ms, the accuracy requirement for measuring ρ is achieved. If a measurement interval of 2.08 ms is used, then a timing error of ≤10 ns is satisfactory. However, for the longer measurement interval it is necessary to reduce the tolerance of the frequency error to ≤6 Hz. We can effectively get a longer measurement interval and avoid the tighter tolerance on frequency error by averaging several measurements, as considered later.

The errors caused in the measurement of ρ_0 by errors in estimating τ_0 and $\Delta\omega$ are presented in Figs. 14a and 14b. The error curves correspond to transmitting an ideal pilot in which the true value of ρ_0 is 1.0. This is the same as the signal model used for the curves in Fig. 13. We see that the errors caused by timing and frequency errors are relatively insensitive to the measurement interval when measuring code-domain power. The reason for this is the difference in the lengths of the correlators used for the code-domain power and waveform quality calculations. For code-domain power, correlated energies are computed over subintervals one Walsh function interval in length and then 20 of these energy computations are averaged in the case of the 1.04-ms measurement interval, or 40 are averaged in the case of the 2.08-ms measurement interval. For the waveform quality calculation, the correlated energy over the entire measurement interval is computed. Because the length of the correlator used for ρ is a factor of 20 or 40 greater than the length used for ρ_i, the measurement of ρ is much more sensitive to uncompensated frequency errors than the measurement of ρ_i.

Fig. 14. *Errors caused in the measurement of ρ_0 by errors in estimating (a) τ_0 and (b) $\Delta\omega$. The error curves correspond to transmitting an ideal pilot in which the true value of ρ_0 is 1.0 (same signal model as for Fig. 13). The results for ρ_i for $i \neq 0$ are essentially the same.*

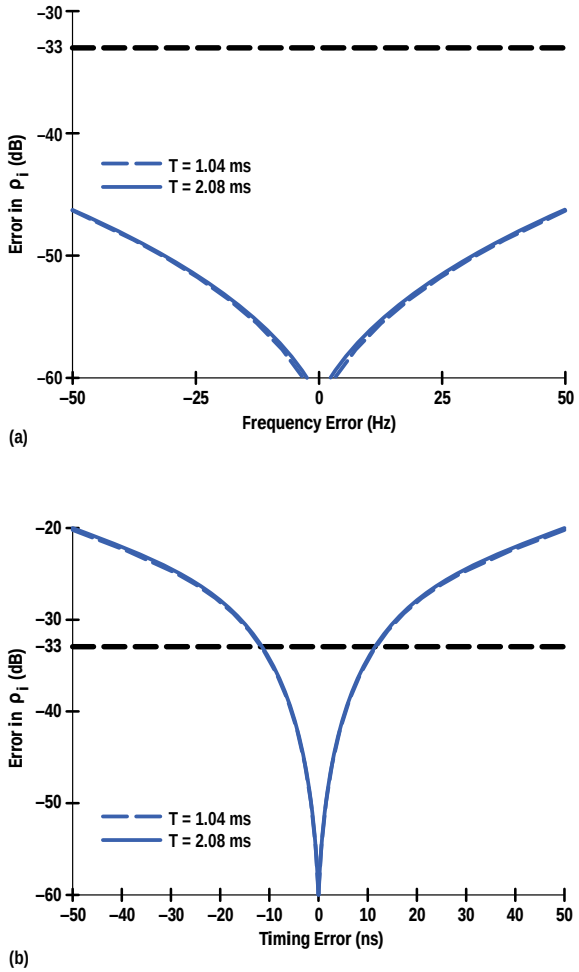

From the error curves in Fig. 14, we see that if the tolerances given by equation 63 are achieved, then the accuracy requirement for ρ_0 given in Table XIV is achieved. Again, as with ρ, the percentage error in measuring ρ_0 is independent of the true value of ρ_0.

The curves in Fig. 14 were obtained for ρ_0. However, since all code channel measurements experience essentially the same sensitivities to timing and frequency errors, these curves apply to any ρ_i, i = 0, 1, ..., 63 within the dynamic range of the equipment.

Since the dynamic range of the code-domain power measurement equipment is approximately 45 dB, precise values of code-domain power, well within the tolerances specified by the IS-97 standard, can be obtained for $\rho_i = 1.0$ to $\rho_i \approx 3.2 \times 10^{-5}$ if the tolerances on the estimates of timing and frequency errors are satisfied. To observe code-domain power to a level of −45 dB, it would be necessary to use a test signal with a waveform quality factor of $\rho \geq 0.99997$, where the errors are uniformly distributed in power over the 64 code channels.

The measurements of ρ and ρ_i may have error components that are random. Moreover, if a sequence of measurements is made from independent data records, then the random errors for the independent records are uncorrelated. To reduce the random error components added to the measurements of ρ and ρ_i, averaging of a set of measurements obtained from the independent records can be performed. To perform this averaging, it is not appropriate to average the values obtained for ρ and ρ_i directly, since this would introduce a bias to the final result. Rather, the energy terms contained in the numerator and denominator of equation 40 for ρ and equation 32 for ρ_i are averaged separately, and then the final values are obtained as the ratios of these averages. This mode is referred to in the HP 83203B as "Fast Code-Domain Power with Averaging."

Accuracy in Measuring $\Delta\tau_i$ and $\Delta\theta_i$. The performance of the algorithms for the code-domain parameter estimator was tested by performing simulations in which Gaussian random errors were added to the simulated transmitting signals. A theoretical expression was derived for the standard deviation of the estimates of phase offsets, $\Delta\theta_i$, based on the same mathematical model used for the simulations. It was found that the results obtained from the simulations agreed very well with the results obtained from the theoretically derived equation, with differences of less than 10 percent. Moreover, it was found that the error in estimating time offsets, $\Delta\tau_i$, when measured in nanoseconds, was approximately one-half the error in measuring phase offsets measured in milliradians. Since the tolerances on measurement accuracy given in Table XIV are ±10 nanoseconds for time offsets and ±10 milliradians for phase offsets, the measurement interval is governed by the accuracy requirement for phase offsets. To measure time offsets and phase offsets to the accuracy specified in the standard, it was found necessary to average subestimates of these parameters. A noteworthy outcome of the performance analysis discussed herein is that the algorithms designed for the code-domain parameter estimator indeed minimize the sum-square difference between the actual transmit signal and the estimated ideal transmit signal, as specified in the IS-97 standard.

The expression derived for the rms error of the estimate of the phase of a code channel is:

$$\sigma_{\hat{\theta}} = \frac{1}{2}\frac{\text{evm}}{\sqrt{\text{BNT}}} \ , \qquad (64)$$

where evm is the *effective* error-vector magnitude, which is equal to the ratio of the total energy of the error divided by the energy of the code channel signal in question, B = 615 kHz is the bandwidth of the baseband transmit signal, T is the measurement interval for one subestimate of the phase, and N is the number of subestimates averaged to obtain the estimate of phase.

The worst case occurs for the sync channel, which for the nominal test model given in Table XIII has 4.71% of the total transmit energy. If the waveform quality factor for each active code channel is $\rho = 0.912$, then the effective evm^2 for the sync channel is given approximately as:

$$\text{evm}^2 = \frac{1/\rho - 1}{0.0471} = 2.049. \qquad (65)$$

If the measurement interval is T = 2.0 ms (2.2 ms was used in the simulations) and the number of subestimates averaged is 34, then the resulting rms error of the estimate of the phase of the sync channel is:

$$\sigma_{\hat{\theta}_{\text{sync}}} = \frac{1}{2}\sqrt{\frac{2.049}{(615)(34)(2.0)}} = 3.50 \text{ mrad.} \qquad (66)$$

The effective evm^2 for the pilot channel is:

$$\text{evm}^2 \approx \frac{1/\rho - 1}{0.2} = 0.4825 \ , \qquad (67)$$

from which, for the same conditions as for the sync channel, we obtain the rms error of the estimate of the phase of the pilot channel as:

$$\sigma_{\hat{\theta}_{\text{pilot}}} = \frac{1}{2}\sqrt{\frac{0.4825}{(615)(34)(2.0)}} = 1.70 \text{ mrad.} \qquad (68)$$

Since the phase offset of the sync channel is:

$$\Delta\hat{\theta}_{sync} = \hat{\theta}_{sync} - \hat{\theta}_{pilot}\ , \qquad (69)$$

and $\hat{\theta}_{sync}$ and $\hat{\theta}_{pilot}$ are uncorrelated,

$$\sigma_{\Delta\hat{\theta}sync} = \sqrt{\sigma^2_{\hat{\theta}sync} + \sigma^2_{\hat{\theta}pilot}} = \sqrt{3.5^2 + 1.7^2} = 3.89 \text{ mrad.} \qquad (70)$$

The estimates of phase are obtained from the sum of 25 subestimates in which the errors in the subestimates are essentially independent. Therefore, the estimate of phase offset is well-approximated as a Gaussian random variable. Using the Gaussian approximation, the 99% confidence interval for the estimate of the phase offset of the sync channel for the nominal test model is:

$$\text{99\% confidence interval} = \pm 2.57\sigma_{\Delta\hat{\theta}sync} = \pm 10 \text{ mrad.} \qquad (71)$$

The measurement accuracy requirement for $\Delta\theta_i$ given in Table XIV is an absolute ±10 milliradians. If we interpret this as the 99% confidence interval, then the accuracy requirement can be achieved by averaging 34 estimates obtained using a 2.0-ms measurement interval as demonstrated by the above example. Other combinations of N and T can be used to achieve the required accuracy, provided that the value of T is not too small to allow acquisition of frequency and timing. It is recommended that a measurement interval of $T \geq 1.0$ ms be used to obtain reliable performance. Other combinations of N and T that will allow measurement errors for $\Delta\theta_i$ of less than ±10 mrad are presented in Fig. 15. As pointed out above, if $\Delta\theta_i$ is measured to the accuracy required, then the accuracy requirement for $\Delta\tau_i$ will also be achieved. We wish to emphasize that the accuracy of the measurements of $\Delta\tau_i$ and $\Delta\theta_i$ depends on the waveform quality and the percentage of power in the code channel being measured. The curves in Fig. 15 represent a worst-case situation in which the waveform quality is $\rho = 0.912$ for all code channels and only 4.71% of the transmitter power is contained in the code channel being measured. For other test models, the lower bounds on NT can be obtained following the example given above and, for larger values of ρ, would be significantly lower than those given in Fig. 15.

Fig. 15. *Lower bounds on NT for $\Delta\theta_i$ measurement errors less than ±10 milliradians for various confidence levels.*

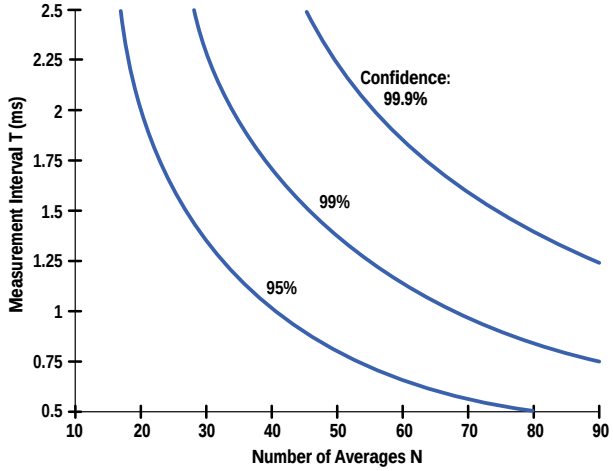

Accuracy in Measuring τ_0 and $\Delta\omega$. The accuracy in measuring ρ and ρ_i is primarily dependent on the accuracy of the estimates of τ_0 and $\Delta\omega$ as shown in Figs. 13 and 14. If τ_0 and $\Delta\omega$ were obtained precisely, then the magnitude of the errors in the values obtained for ρ and ρ_i would be less than 10^{-4}, which is well within the accuracy specified for the HP 83203B.

The best accuracy for the estimates of τ_0 and $\Delta\omega$ is obtained when the full parameter estimator is employed to estimate the time and phase offsets of code channels. In this case, τ_i and θ_i are determined for all active code channels and the estimate of $\Delta\omega$ is obtained jointly with the estimates of τ_i and θ_i.

The next best accuracy for the estimates of τ_0 and $\Delta\omega$ is obtained by using a reference signal synthesized as the sum of the reference signals for all active code channels, as is done for the full parameter estimator, but with the time and phase offsets set equal to zero in the parameter estimator. This procedure reduces the search for phase and timing from a 2K-dimensional problem, where K is the number of active code channels, to a 2-dimensional problem.

The accuracy of the estimates of τ_0 and $\Delta\omega$ was determined through simulations in which the nominal signal model was used with random time and phase offsets introduced to the code channels and a measurement interval of 1.09 ms. Timing and phase offsets that were uniformly distributed over a range of ±50 ns for time offsets and ±50 mrad for phase offsets were introduced. The results of these simulations are presented in Figs. 16 and 17, which show the rms errors of the estimates of τ_0 and $\Delta\omega$, respectively, as functions of ρ.

Fig. 16. *Rms error of the estimate of τ_0 as a function of signal quality ρ, determined through simulations in which the nominal signal model was used with random time offsets of 0 to ±50 ns and phase offsets of 0 to ±50 mrad introduced to the code channels and a measurement interval of 1.09 ms.*

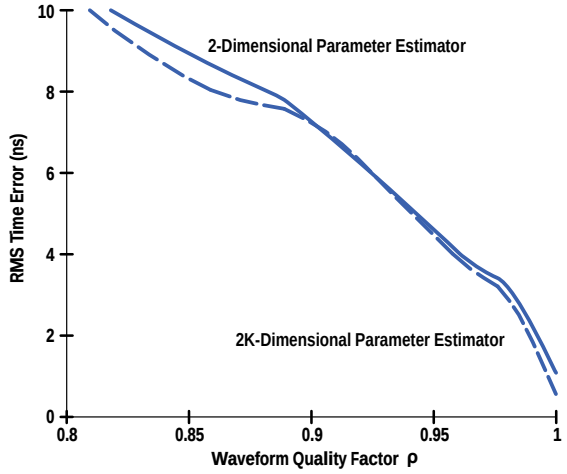

Fig. 17. *Rms error of the estimate of $\Delta\omega$ as a function of signal quality ρ, determined through simulations using the same signal model as for Fig. 16.*

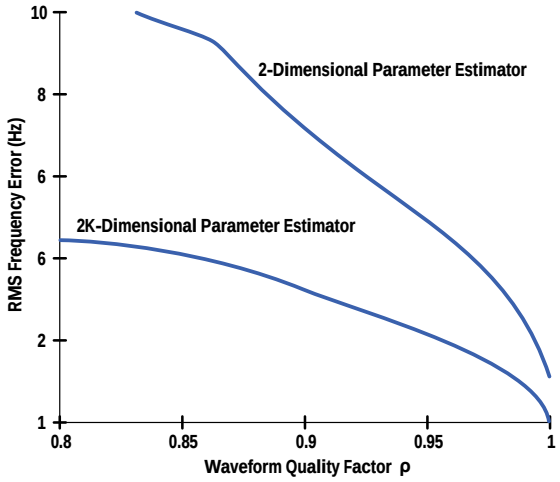

From Fig. 16, we see that the estimates of τ_0 obtained from the 2-dimensional parameter estimator are nearly as accurate as those obtained from the full 2K-dimensional parameter estimator. On the other hand, we see from Fig. 17 that the full parameter estimator provides roughly a factor of two less error in estimating frequency compared to the 2-dimensional parameter estimator. These curves show that there is little advantage in using the full parameter estimator unless time and phase offsets are outputs of the measurement. Therefore, the second method of obtaining estimates of τ_0 and $\Delta\omega$ is recommended when measuring code-domain power without measuring time and phase offsets. A mode in the HP 83203B referred to as "Accurate Code-Domain Power" employs this second method of obtaining estimates of τ_0 and $\Delta\omega$.

The third method for obtaining estimates of τ_0 and $\Delta\omega$ uses a reference signal consisting of only the pilot signal. This mode is referred to as "Fast Code-Domain Power" in the HP 83203B. If only the pilot channel is transmitted, then this mode is as accurate as the other two and is appropriate for measuring code-domain power. Moreover, if τ_0 and $\Delta\omega$ are known a priori, then the "Fast Code-Domain Power" mode should be used.

Presented in Fig. 18 are curves obtained from simulations showing the rms error in estimating τ_0 and $\Delta\omega$ for the case in which only the pilot channel is transmitted and a measurement interval of 1.09 ms is used. Curiously, these curves show that the timing errors in ns and the frequency errors in Hz are nearly identical. If we assume that the measurement errors are Gaussian, then we can obtain the 99% confidence limits for the measurement of τ_0 and $\Delta\omega$ by multiplying the rms values given in Fig. 18 by a factor of 2.57. To obtain the measurement error of less than ±10 ns for τ_0 and less than ±10 Hz for $\Delta\omega$ as specified in Table XIV with a confidence of 99%, the rms errors in measuring τ_0 and $\Delta\omega$ must be less than 3.9 ns for τ_0 and less than 3.9 Hz for $\Delta\omega$. From Fig. 18, we see that τ_0 and $\Delta\omega$ can be estimated to sufficient accuracy for $0.85<\rho<1.0$ using a measurement interval of 1.09 ms. This exceeds the range of $0.9<\rho<1.0$ specified in Table XII.

Referring to the performance curves in Figs. 16 and 17, we see that if ρ is less than approximately 0.97, then the performance given by these curves may not be adequate. If it is necessary to obtain better estimates of τ_0 and $\Delta\omega$ than those

given in Figs. 16, 17, and 18, then it will be necessary to use a longer measurement interval than the 1.09 ms considered here, or to average estimates obtained from independent time records, as is done for the time and phase offset measurements. As for the time and phase offset estimates, the rms errors of the estimates of τ_0 and $\Delta\omega$ are proportional to $1/\sqrt{NT}$.

Fig. 18. *Curves obtained from simulations showing the rms error in estimating τ_0 and $\Delta\omega$ for the case in which only the pilot channel is transmitted and a measurement interval of 1.09 ms is used.*

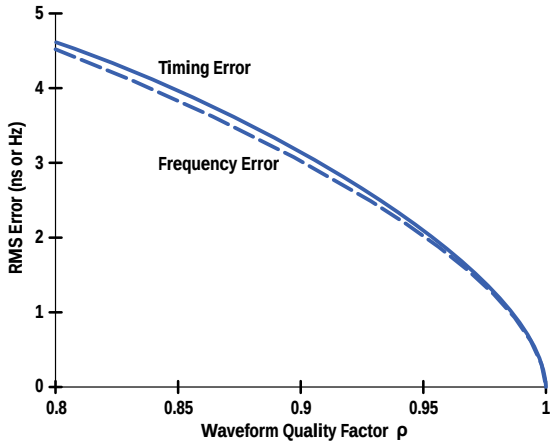

Measurement Examples

Typical results obtained with the HP 8921A cell site test set using the HP 83203B measurement algorithms are presented in Figs. 19 and 20. These results are not intended to validate any particular base station, but are presented only to illustrate actual measurements obtained using the algorithms discussed in this paper. The results presented in Fig. 19 were obtained from a base station transmitter in which the pilot, paging channel 1, sync channel 32, and one full-rate traffic channel 11 were active. From Fig. 19a, we see that the floor of the code-domain power is at approximately –38 dB relative to the total transmitter power which corresponds to a relative error energy level of –38 dB + 18 dB = –20 dB. The factor of 18 dB corresponds to the distribution of energy to 64 code channels. The floor level of –38 dB corresponds to a value of ρ approximately equal to:

$$\rho \approx \frac{1}{1 + 10^{-2.0}} = 0.9901. \qquad (72)$$

The value of ρ measured was 0.9882. From the measured value of ρ we can calculate the approximate value of the floor level of the code-domain spectrum as:

$$\begin{aligned}\text{Floor Level} &\approx 10\log_{10}(1/\rho - 1) - 18 \\ &= -37.23 \text{ dB},\end{aligned} \qquad (73)$$

which agrees closely with the floor level we see in Fig. 19a.

From the plot of code-domain power in Fig. 19a, we see that code channel 33 is significantly above the floor, even though code channel 33 was not active. This is an indication that the active code channels were leaking energy into code channel 33. It should be pointed out that the base station was overdriven during this measurement, which could be seen from a measurement of the spectrum of the transmitted signal. The plot of the measured spectrum is not included in this paper.

Measurements of time offsets and phase offsets obtained for a measurement interval of 1.25 ms are presented in Figs. 19b and 19c. For these measurements no averaging was used; therefore, the value of NT to use in equation 64 to determine the accuracy of the measurement is NT = 1.25 ms. The channel with the smallest energy level was the sync channel 32 for which the relative measured energy level was –12.8 dB. This corresponds to 5.25% of the energy in the sync channel. By using equation 65 with ρ = 0.9882, we obtain an effective evm^2 for the sync channel of:

$$\text{evm}^2 = \frac{1/\rho - 1}{0.0525} = 0.227. \qquad (74)$$

Using this value in equation 64, we obtain for the rms error of the estimate of the phase of the sync channel:

$$\sigma_{\hat{\theta}\text{sync}} = \frac{1}{2}\sqrt{\frac{0.227}{(615)(1.25)}} = 8.6 \text{ mrad}. \qquad (75)$$

The relative power in the pilot channel was –1.41 dB which corresponds to 7.73% of the total energy in the pilot. By following the above procedure for the pilot channel, we obtain the rms error for the estimate of the phase of the pilot channel:

Fig. 19. *Results of code-domain measurements of a base station transmitter with the pilot (0), paging channel (1), sync channel (32), and one full-rate traffic channel (11) active. (a) Code-domain power measurements. (b) Time offset measurements. (c) Phase offset measurements.*

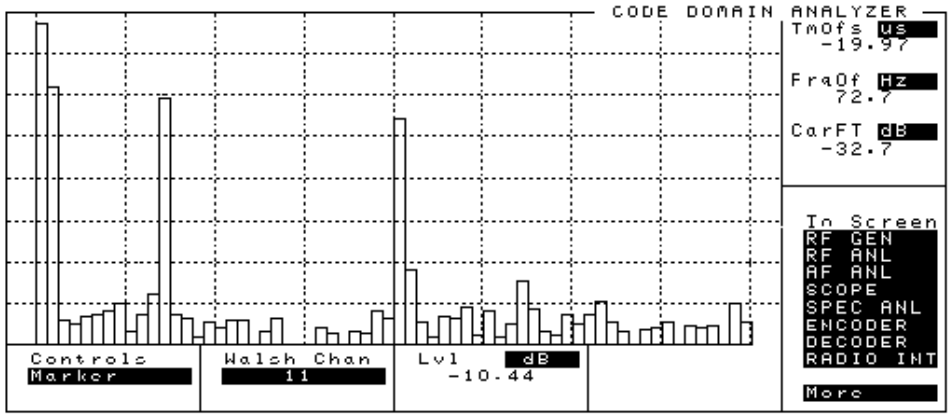

(a)

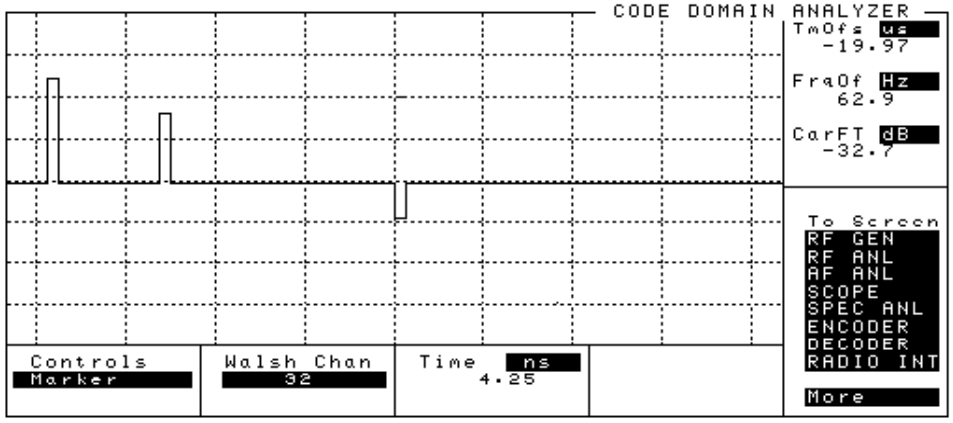

(b)

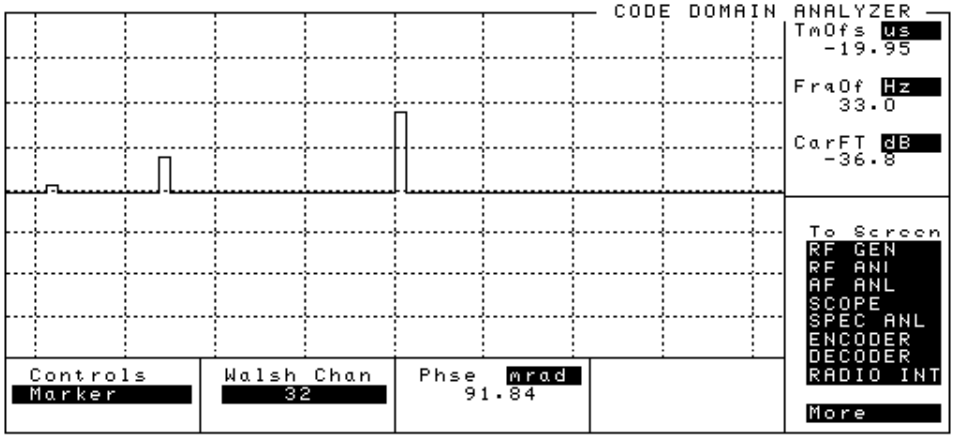

(c)

$$\sigma_{\hat{\theta}_{pilot}} = 7.3 \text{ mrad.} \qquad (76)$$

Using the rms errors obtained above in equation 70, we obtain the rms error in the measurement of the phase offset of the sync channel:

$$\sigma_{\hat{\theta}_{sync}} = \sqrt{8.6^2 + 7.3^2} = 11.3 \text{ mrad.} \qquad (77)$$

and by using the Gaussian assumption used for equation 71 we obtain:

Fig. 20. *Results of code-domain measurements of a base station transmitter with the pilot (channel 0), paging channel (1), sync channel (32), and four full-rate traffic channels (5, 6, 7, 8) active. (a) Code-domain power measurements. (b) Time offset measurements. (c) Phase offset measurements.*

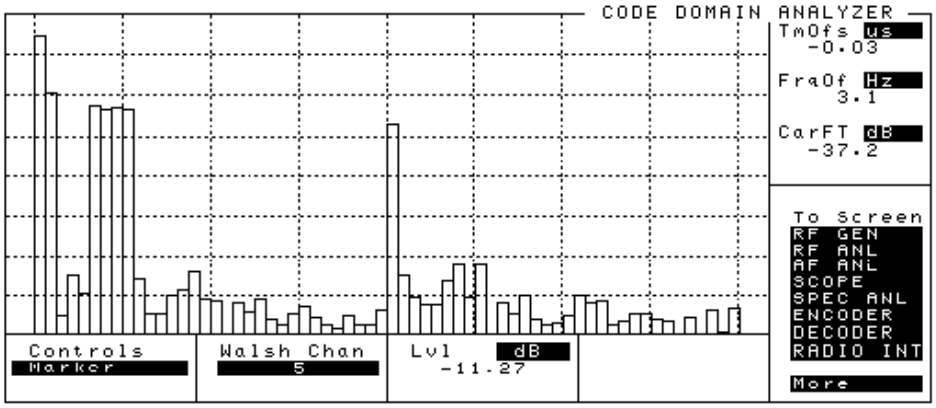

(a)

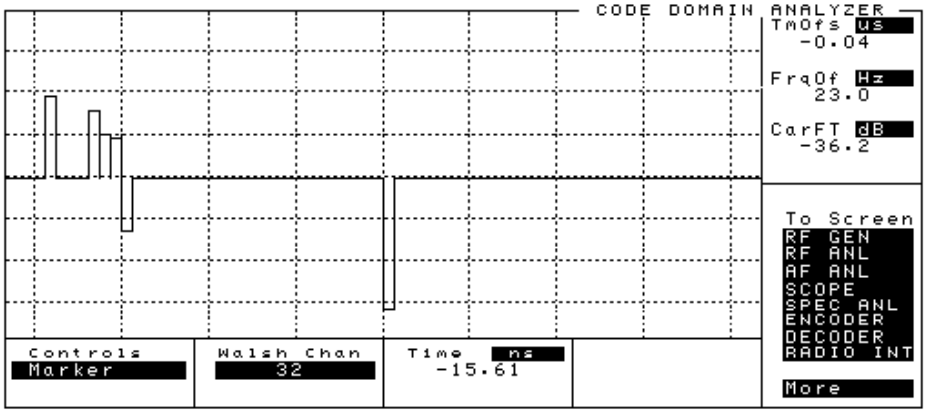

(b)

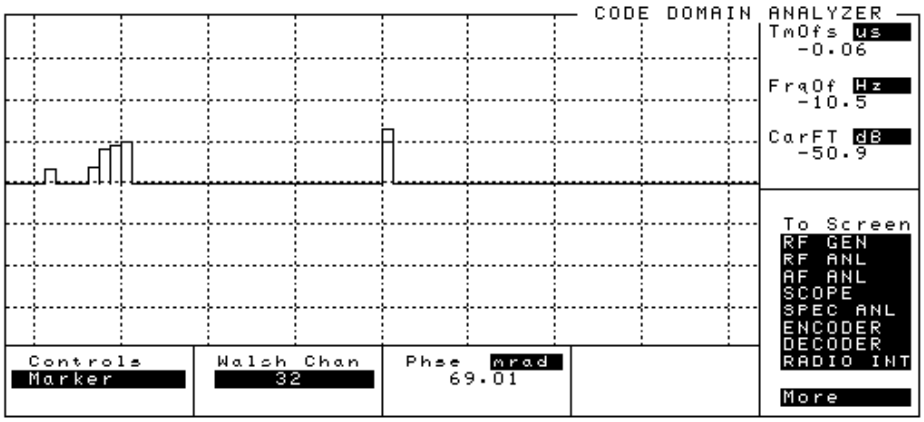

(c)

$$99\%\ \text{confidence interval} = \pm 2.57\sigma_{\Delta\hat{\theta}\text{sync}} = \pm 29\ \text{mrad}. \quad (78)$$

Thus, from the results of the simulations discussed previously, we can expect a 99% confidence interval for the measurement of time offset of approximately ±14.5 ns.

From Fig. 19b, we see that the measured time offsets are within the ±50-ns tolerance given in the IS-97 standards, with the worst-case 17-ns time offset occurring for the paging channel. The time offset specification is satisfied even if we include the ±14.5-ns confidence interval. From Fig. 19c, we see that the phase offsets for the sync channel and the traffic channel

are well within the ±50-mrad tolerance given by the standard. However, the measured phase offset for the traffic channel was 91.8 mrad, which is outside the tolerance specified by the standard.

For the time and phase offset measurements presented here, the confidence intervals for the measurements were larger than could be used for valid tests. As discussed in the section on accuracy above, to obtain acceptable measurement accuracy it is necessary to average estimates of time and phase offsets. For the measurement situation of Fig. 19, acceptable measurement accuracy would have been achieved by averaging nine estimates to reduce the measurement confidence intervals by a factor of 3.

The results of the code-domain measurements of a base station transmitter in which four full-rate code channels 5, 6, 7, and 8 are active are presented in Fig. 20. In this case, we see that a significant amount of energy is leaked to inactive code channels. From Figs. 20b and 20c, we see that the largest time offset and phase offset are –15.6 ns and 69 mrad, respectively, for the sync channel. For these results, a single measurement interval of 1.25 ms was used, which results in large measurement confidence intervals.

Acknowledgments

The author wishes to acknowledge Marcus DaSilva, who led the HP 83203B project, and thank him for his continual support and enthusiasm during the development of the CDMA measurement algorithms, for encouraging the writing of this paper, and for carefully reviewing an early draft, including the meticulous checking of the numbers presented in the examples. Thanks also to Dave Whipple, who served on the IS-95 and IS-97 standards committees and contributed to the concepts of measuring waveform quality factor ρ and code- domain power ρ_i, for his support during the development of the CDMA measurement algorithms. Special thanks to Michael McNamee, who developed the data acquisition subsystem for the HP 83203B and ported the C code for the measurement algorithms from the development platform to the HP 83203B signal processing platform. Special thanks also to Tom Yeager, who performed field tests and demonstrations and obtained the bitmaps of the measurement results presented in this paper. The author also wishes to thank Michael McNamee, Tom Yeager, Dave Hoover, and Matt Hunton for reviewing this paper and providing some helpful suggestions.

Reference

D.P. Whipple, “North American Cellular CDMA,” *Hewlett-Packard Journal*, Vol. 44, no. 6, December 1993, pp. 90–97.

▶ Go to Table of Contents
▶ Go to HP Journal Home Page